



HAL
open science

Potassium distribution and isotope composition in the lithospheric mantle in relation to global Earth's reservoirs

Dmitri Ionov, Kun Wang

► **To cite this version:**

Dmitri Ionov, Kun Wang. Potassium distribution and isotope composition in the lithospheric mantle in relation to global Earth's reservoirs. *Geochimica et Cosmochimica Acta*, 2021, 309, pp.151-170. 10.1016/j.gca.2021.06.033 . hal-03400301

HAL Id: hal-03400301

<https://hal.science/hal-03400301>

Submitted on 2 Aug 2023

HAL is a multi-disciplinary open access archive for the deposit and dissemination of scientific research documents, whether they are published or not. The documents may come from teaching and research institutions in France or abroad, or from public or private research centers.

L'archive ouverte pluridisciplinaire **HAL**, est destinée au dépôt et à la diffusion de documents scientifiques de niveau recherche, publiés ou non, émanant des établissements d'enseignement et de recherche français ou étrangers, des laboratoires publics ou privés.



Distributed under a Creative Commons Attribution - NonCommercial 4.0 International License

Potassium distribution and isotope composition in the lithospheric mantle in relation to global Earth's reservoirs

Dmitri A. Ionov^{a*}, Kun Wang^b

^a *Géosciences Montpellier, Université de Montpellier, 34095 Montpellier, France*

^b *Department of Earth and Planetary Sciences and McDonnell Center for the Space Sciences,
Washington University in St. Louis, St. Louis, MO 63130, USA*

**Corresponding author: dionov@umontpellier.fr (D.A. Ionov)*

ABSTRACT (420 words)

Recent analytical advances have provided means to measure potassium (K) isotopes in various terrestrial materials, but little is known about K distribution and stable isotope composition in the lithospheric mantle because of: (a) common low K abundances, (b) potential contamination and alteration, (c) diversity of mantle rocks and minerals hosting K in different tectonic settings. We report K abundances and $\delta^{41}\text{K}$ values for well-studied whole-rock (WR) mantle xenoliths (spinel and garnet peridotites and pyroxenites) from mobile belts, a craton, a subduction zone, as well as for K-rich phases (mica, amphibole, silicate glass) and xenolith-bearing volcanic materials (67 samples). The xenolith materials show extremely broad ranges of K content (7 $\mu\text{g/g}$ to 6.6 wt.%) and $\delta^{41}\text{K}$ (-2.77‰ to 0.62‰). They contrast with the narrow $\delta^{41}\text{K}$ range for host volcanic materials (-0.53‰ to -0.27‰) and literature data on oceanic basalts (melting products of upwelling asthenosphere: $-0.43 \pm 0.17\text{‰}$, 2sd). Amphibole-bearing subduction zone peridotites show the highest WR $\delta^{41}\text{K}$ values (0.40 to 0.62‰) likely inherited from fluids released into the mantle wedge from subducted oceanic crust. All other WR samples yield negative $\delta^{41}\text{K}$: -0.06‰ to -2.77‰ for peridotites and -0.17‰ to -0.52‰ for pyroxenites. The $\delta^{41}\text{K}$ in K-rich mantle phases range from positive values (0.16 to 0.57‰) for phlogopite in strongly metasomatized peridotites to negative values (-0.27 to -0.94‰) for phlogopite, amphibole and glass pockets from other samples, which cannot be explained by equilibrium inter-mineral fractionation inferred from ab initio calculations. We attribute the broad $\delta^{41}\text{K}$ variations to (a) isotope fractionation during fluid-rock interaction in the mantle, and (b) distinct sources of K-bearing fluids. Kinetic isotope fractionation during fluid percolation and diffusion is inferred for composite xenoliths (phlogopite and pyroxenite veins in peridotites) that have lower $\delta^{41}\text{K}$ in the hosts than in the veins due to slower migration of ^{41}K than ^{39}K from the veins (former fluid channels) to host mantle. Overall, the K isotope fractionation in the lithospheric mantle appears to be greater than for magmatic fractionation in the crust. The average $\delta^{41}\text{K}$ of normal off-craton continental lithospheric mantle calculated from the least altered fertile and lightly metasomatized lherzolites is $-0.57 \pm 0.28\text{‰}$ (2sd). This value is within error (though a little lower) of estimates for both continental crust and MORB and OIB mantle sources indicating that these major silicate Earth reservoirs

have similar bulk $\delta^{41}\text{K}$ values, apparently due to low or negligible K isotopic fractionation during their formation by magmatic differentiation and melting. By contrast, K isotopes in modern and fossil subduction zones are fractionated via fluid-related equilibrium and kinetic processes.

Keywords: potassium; K isotope; stable isotope fractionation; lithospheric mantle; mantle xenolith; metasomatism; phlogopite

9789 words, 1 table, 5 figures, 112 references; 4 electronic supplements

1. Introduction

1.1 Potassium and its isotopes in Earth's reservoirs

Potassium (K) is a volatile, lithophile alkali metal, which strongly fractionates from solids to magmatic liquids and fluids. The K content [K] of the Bulk Silicate Earth (BSE), inferred from estimates of K/U ratio in its major reservoirs, is $280 \pm 120 \mu\text{g/g}$ (2σ) (Arevalo et al., 2009; McDonough et al., 1992). About a third of the total K may reside in the continental crust (CC) that makes up $<0.6\%$ of the mass of the BSE, but contains as much as 15,000–17,000 $\mu\text{g/g}$ K. The mantle sources of the mid-ocean ridge and ocean island basalts (MORB and OIB) are estimated to contain ~ 100 and $\sim 480 \mu\text{g/g}$ K, respectively. The K distribution in the lithospheric mantle has not been thoroughly examined and is poorly constrained.

Potassium has two stable isotopes, ^{39}K (93.2581%) and ^{41}K (6.7302%), and one radioactive isotope ^{40}K (0.0117%) with a half-life of 1.277×10^9 years. K isotope analyses were problematic until recent development of high-precision analytical methods enabled to resolve K isotopic variations ($^{41}\text{K}/^{39}\text{K} < 0.1\%$) in geologic materials and processes (e.g. Hu et al., 2018; Li et al., 2016; Morgan et al., 2018; Wang and Jacobsen, 2016), which prompted studies of various crustal materials (e.g. Huang et al., 2020; Sun et al., 2020).

Potassium is fluid-mobile, and a sensitive indicator of water-rock exchanges, e.g. during seafloor hydrothermal alteration. Recent work (Wang et al., 2020) has found significant K isotope offset between fresh oceanic basalts and seawater ($\sim 0.6\%$ in $\delta^{41}\text{K}$ values) which opens a potential to use K isotope data to trace the cycling of K from near-surface to deep geologic reservoirs (Li et al., 2019a; Li et al., 2016; Liu et al., 2020; Morgan et al., 2018; Parendo et al., 2017; Santiago Ramos et al., 2020; Wang and Jacobsen, 2016).

The composition of the Earth's upper mantle is commonly inferred from studies of fragments (xenoliths) of mantle rocks carried to the surface by volcanic eruptions (Maaloe and Aoki, 1977; McDonough, 1990; Palme and O'Neill, 2003). This approach, however, is problematic for K and other highly incompatible trace elements, whose extraction from the BSE to the crust has dramatically reduced their abundances in the residual mantle (Hofmann, 1988). Constraining K isotope composition of residual mantle peridotite xenoliths is challenging due to a combination of low K and potential contamination. This is why the K

isotope estimates for generic upper mantle were initially obtained from data on oceanic basalts, i.e. mantle melting products (Hu et al., 2021b; Tuller-Ross et al., 2019a; Wang and Jacobsen, 2016) These magmas, however, are generated in the asthenosphere, and give no information on the lithospheric mantle. Further, they provide averaged sampling of their sources, and convey little evidence on mantle heterogeneity.

1.2 Potassium in the upper mantle

Potassium is highly incompatible in peridotites, the most common upper mantle rocks consisting of magnesian olivine, pyroxenes and spinel or garnet. Melt extraction from the BSE early in the Earth's history took out much K to proto-crust and thus markedly reduced its concentration in the remaining material, i.e. depleted convecting mantle, the source of MORB (Hofmann, 1988). Subsequent recurring melting of the asthenosphere left behind solid residues, even more depleted in K, that accumulated to form continental lithospheric mantle (CLM). However, parts of the initially melt-depleted, hence K-poor, lithospheric mantle were later metasomatized, i.e. transformed by additions of (and/or reaction with) different melts and fluids (e.g. Bodinier et al., 1990; Frey and Green, 1974; Lloyd and Bailey, 1975; Menzies and Hawkesworth, 1987). These metasomatic media are usually enriched in incompatible elements including K and may originate from multiple sources such as asthenosphere, mantle plumes and recycled surface materials.

The sum of these processes over billions of years has produced a CLM with highly heterogeneous K distribution. The K concentrations in mantle regions that experienced little or no metasomatism are generally low (<100 ppm, e.g. Ionov et al., 1992a; Wiechert et al., 1997), but CLM portions enriched by metasomatism may show broad K variations caused by, first, the composition of incoming metasomatic media, and second, the way they interact with the host mantle (e.g. Bodinier et al., 1990). The simplest interaction model is mixing of depleted mantle with trapped portions of percolating melt or fluid, which then solidify in situ (Frey and Green, 1974). Alternatively, a mantle rock may equilibrate with a continuous flow of percolating melt in line with partition coefficients of each element. This may lead to either melt-solid elemental exchange with existing mantle minerals (cryptic metasomatism) or formation of new metasomatic phases (modal metasomatism) due to melt-rock reaction

(Dawson, 1982; Menzies et al., 1985; Roden and Murthy, 1985) usually inside and close to melt channels (e.g. Bodinier et al., 2004; Nielson et al., 1993).

In most cases, however, the metasomatic processes appear to be more complex, with modal metasomatism and near-equilibration with metasomatic media close to melt feeders and the entrapment of evolved, small-volume residual fluids far from the feeders recorded in composite xenoliths (mafic veins in peridotites) (Irving, 1980) and peridotite massifs (e.g. Bodinier et al., 1990). Such processes may be accompanied by ‘chromatographic’ evolution of the composition of percolating media with the distance from the melt conduits, controlled by element partition coefficients and modal abundances in host rocks, with enrichments in highly incompatible (e.g. K) relative to more compatible elements away from the source (e.g. Bodinier et al., 2004; Navon and Stolper, 1987).

Metasomatic enrichments may also depend on the type of metasomatic fluids, usually ‘carbonatitic’ vs. ‘silicate’ (e.g. Yaxley et al., 1998), yet chromatographic models imply continuous evolution from CO₂-bearing silicate melts in the source (magma feeder) to carbonate-rich fluids at the percolation front due to melt-host reactions (e.g. Bodinier et al., 2004). Another important aspect of metasomatism is its tectonic setting, which controls the provenance, hence chemical and isotope composition, of metasomatic media. The sources of intra-plate metasomatism are believed to be linked to asthenospheric upwelling or deep-mantle plumes whereas in subduction zones they are related to recycling of crustal materials (e.g. Hofmann, 1997).

Modal metasomatism may precipitate K-rich phases, mainly phlogopite (phl, ~8–10% K₂O) and amphibole (amph, 0.1–2% K₂O) (e.g. Dawson and Smith, 1982; Delaney et al., 1980; Grégoire et al., 2002; Ionov et al., 1997; Nielson et al., 1993) as well as alkali feldspars (0.2–11% K₂O) (Ionov et al., 1999; Ionov et al., 1995; Xu et al., 1996), quenched glass (e.g. Chazot et al., 1996; Ionov et al., 1994; Xu et al., 1996; Zinngrebe and Foley, 1995) and K-bearing clinopyroxene (cpx) in high-pressure rocks (Wang and Takahashi, 1999).

CLM materials can be sampled in tectonically emplaced massifs or as fragments (xenoliths) hosted by volcanic rocks (e.g. Palme and O'Neill, 2003). Massif peridotites provide large samples and enable to observe relations of different rock types, but they are usually overprinted by metamorphism during their emplacement at plate margins involving

formation of K-bearing minerals, and may be affected by weathering. By contrast, mantle xenoliths are transported to or near the surface very rapidly (hours to days), and those from recent eruptions are not, or little, altered. However, care should be taken to ensure that xenoliths are not contaminated by K-rich host magmas.

The distribution of K in the CLM is poorly constrained because of common inadequate sampling (altered or magma-contaminated samples) and/or analytical problems at low [K]. Major oxide analyses are usually done by methods with detection limits at or above the K content in common mantle rocks (peridotites, pyroxenites). Routine ICP-MS analyses are affected by interference from ^{40}Ar . As a result, K abundances reported for many mantle xenoliths are inexact, and averages in data compilations may be fairly high (e.g. Palme and O'Neill, 2003). Better results are obtained by flame photometry, ICP-AAS or ICP-AES; they show that fresh, non-metasomatized peridotites contain $\leq 100 \mu\text{g/g}$ K, often as little as 10–20 $\mu\text{g/g}$ (e.g. Ionov et al., 1992a; Wiechert et al., 1997).

To sum up, constraining K-isotope variations in the lithospheric mantle necessitates analyses of large numbers of different samples in order to represent: (a) variably melt-depleted peridotites; (b) rocks affected by multiple types and degrees of metasomatism; (c) K-bearing metasomatic phases either disseminated in mantle rocks or forming veins and pockets; (d) main tectonic settings: cratons, mobile belts, subduction zones. It is essential to avoid contamination of xenoliths by K-rich materials from host magmas and weathering.

In this study, we report K concentrations and isotope values for 67 geographically diverse, mantle-derived samples including 35 whole-rock (WR) peridotites, three WR pyroxenites, two WR pyroxenite veins and a phlogopite-rich vein as well as their host peridotites from three composite xenoliths, 18 samples of phlogopite, amphibole and glass pockets separated from xenoliths, three WR volcanic rocks that host mantle xenoliths as well as a lower crustal granulite (Table 1). Photographs of selected xenoliths, their portions used to produce WR powders as well as thin section images are given in Electronic Supplement 1 (ES1). Literature data on chemical compositions of the WR peridotites are summarized in Electronic Supplement 2 (ES2), isotope compositions are given in Electronic Supplement 3 (ES3). Our objectives are to constrain K-isotope compositions in the CLM including major

rock types and tectonic settings, and to examine how K isotopes could be used to gain insights into metasomatism, crustal recycling and other mantle processes.

2. Samples

2.1 Sampling localities, geological background and rock types

Many xenoliths in this study were collected in Siberia and Mongolia. This vast area comprises the Siberian craton (e.g. Ionov et al., 2018), the Central Asian Orogenic Belt (CAOB) between the Siberian and North China cratons including the Baikal region (Carlson and Ionov, 2019; Ionov et al., 1992a), far eastern Russia (Ionov et al., 1999) and the Kamchatka peninsula on the subduction-related Pacific coast of Asia (Ionov, 2010). A few samples are from the Eifel volcanic field in Germany and the Gnotuk maar in southeastern (SE) Australia. The xenoliths are hosted by kimberlites on the Siberian craton, andesites in the Kamchatka arc, and Cenozoic alkali basaltic rocks in off-craton localities; the latter formed due to continental extension and mantle convection induced by plate movements and subduction (e.g. Sun et al., 2020).

A major advantage of the xenolith suites from the CAOB is that they have a large proportion of fertile lherzolites with modal and major element compositions similar to those in the BSE estimates, which is also referred to as primitive mantle (PM) in xenolith studies (Hart and Zindler, 1986; Hofmann, 1988; McDonough and Sun, 1995; Press et al., 1986). Lherzolites ($\geq 5\%$ cpx) are the most common rocks in the oceanic and off-craton continental upper mantle; they are subdivided, based on coexisting Al-rich phases, into spinel (≤ 60 km), garnet-spinel (~ 60 – 100 km) and garnet (> 100 km) depth facies (e.g. Ziberna et al., 2013). Fertile spinel lherzolites from Tariat in central Mongolia are compositionally similar to the sources of MORB volcanism (Carlson and Ionov, 2019); large, unaltered Tariat lherzolites as well as garnet-spinel lherzolites from Vitim in southern Siberia (Ionov et al., 2005a) were used to estimate the PM composition (e.g. Palme and O'Neill, 2003).

Harzburgites ($< 5\%$ cpx) are the most common rocks in the cratonic and subduction zone mantle, but are less abundant than lherzolites in the off-craton CLM; they are usually metasomatized (Roden and Murthy, 1985). The distinctive feature of andesite-hosted Kamchatka harzburgites is a combination of variable but commonly high modal

orthopyroxene (opx, 18–30%) with low modal cpx (1.5–3%) and amphibole ($\leq 1\%$). At a given olivine or MgO content, they have higher opx and SiO₂, and lower cpx (as well as Al₂O₃ and CaO) than typical refractory peridotite xenoliths in continental basalts, which indicates fluid fluxing during melting in the mantle wedge (Bénard et al., 2021).

Our collection also includes well-studied, variably metasomatized mantle xenoliths (see Section 1.2) ranging from widespread phl- and amph-bearing peridotites (Ionov et al., 1992b; Ionov et al., 1997) to rarer samples with alkali feldspar (Ionov et al., 1999; Ionov et al., 1995), silicate glass (Ionov et al., 1994), carbonates (Ionov et al., 2018) and various veins (Ionov et al., 1997; Ionov et al., 1998). Amphibole (usually pargasite, e.g. McNell and Edgar, 1987) is the most common accessory volatile- and K-bearing mineral in off-craton lherzolites (Roden and Murthy, 1985). It occurs as discrete grains, grain clusters or intermittent thin veins, sometimes accompanied by phlogopite, which is the most K-rich mineral in the mantle. Spinel peridotite xenoliths containing alkali feldspars have been reported from mobile belts, continental margins and ocean islands, yet are often overlooked.

Overall, the xenolith suite in this study enables assessment of the K content and isotope composition in major rock types and tectonic settings of the CLM (Ionov et al., 1997) except the MARID type xenoliths in South African kimberlites (Dawson and Smith, 1977; Grégoire et al., 2002). Some of these samples were earlier used to assess the isotope composition of Li, Mg, Ca, Cr, Fe, Ni and Zn in the CLM (see ES3 for references).

2.2 Sample preparation

Samples for this study were chosen among xenoliths and related volcanic materials that had been comprehensively studied previously including petrography, modal, chemical and isotope compositions. We used representative and contamination-free WR powders obtained from homogeneous and sufficiently large samples (see ES1 for examples). Mantle xenoliths were sawn to remove the rinds (that may contain volcanic materials and alteration products). Selected least altered material (≥ 100 g; ES1) was crushed by hammer in plastic sheets, and aliquots ground to powder in agate for WR analyses. Pure minerals were handpicked, in some cases from magnetically enriched fractions. Essential petrologic and chemical information on the samples is given in Table 1.

3. Methods

Sample digestion, column chemistry and isotopic analyses were carried out in a Class 10,000 clean lab at the Isotope Cosmochemistry Laboratory, Washington University in St. Louis. Details of the analytical procedures are given in Chen et al. (2019) and in Electronic Supplement 4 (ES4). Depending on previously analyzed K concentrations, 1–600 mg of powdered samples was digested with concentrated HF-HNO₃ acid mixtures (3:1) using Parr high-pressure digestion vessels at 180°C in a Quincy Lab Model 10 lab oven for two days. Samples were then fully dried down under heat lamps and re-dissolved with HCl-HNO₃ acid mixtures (3:1) for two more days. Fully dissolved samples were dried down and refluxed with 0.7 M HNO₃ before loading onto K separation columns. The separation chromatography followed the protocols first described by Strelow et al. (1970). Two columns were used (big and small) filled with 17 mL and 2.4 mL BioRad AG50-X8 100-200 mesh cation-exchange resin, respectively (Chen et al., 2019). Samples were eluted and K-cuts were collected with 0.7 M or 0.5 M HNO₃ for the big and small columns, respectively. Low-K bulk samples were passed through the small column twice in order to further remove matrix elements (Chen et al., 2019). Aliquots of sample solutions after columns (K-cuts) were first analyzed with an iCapQ quadrupole ICP-MS (Thermo Scientific, Bremen, Germany) to determine if any matrix elements remained in the solution. Pre-cuts and post-cuts were also collected at each column and analyzed with the iCapQ to monitor any K loss during column chemistry. Our total procedure blank is 13 ng (Liu et al., 2020), which is negligible compared to K mass in all the samples.

Using the [K] values obtained with iCapQ quadrupole ICP-MS, each sample was diluted to 300 ng/ml to match the [K] of the bracketing standard (NIST SRM 3141a) and measured with the Neptune Plus MC-ICP-MS (Thermo Scientific, Bremen, Germany). Samples were introduced into the MC-ICP-MS with an APEX Omega high sensitivity de-solvation system (Elemental Scientific, Omaha, USA). The typical settings and parameters on Neptune Plus and APEX Omega are shown in ES3. Each sample was analyzed 5 to 22 times using standard-sample-standard technique; number of analyses and average values for each sample are reported in Table 1. The K isotope compositions are

expressed using the per mil (‰) notation $\delta^{41}\text{K}$, where $\delta^{41}\text{K} = [(^{41}\text{K}/^{39}\text{K})_{\text{sample}} / (^{41}\text{K}/^{39}\text{K})_{\text{NIST SRM3141a}} - 1] \times 1000$. The internal (within-run) reproducibility is shown for each sample in Table 1; uncertainties are reported as 2 standard deviations (2sd). The long-term (20 month) external reproducibility, evaluated with reference material BHVO-2, is $\pm 0.11\%$ (2sd) (Chen et al., 2019). BHVO-2 was also run in each analytical session with the samples in this study for quality control; the values, listed in ES4, agree well with literature data (Chen et al., 2019; Hu et al., 2018; Li et al., 2016; Morgan et al., 2018; Wang and Jacobsen, 2016).

Our laboratory routinely measures low-K samples with [K] comparable to those in non-metasomatized peridotites in this study. Our results on USGS reference material BIR-1 (Icelandic basalt) with [K] $\sim 0.025\%$ (-0.51 ± 0.06 , $n = 9$; Chen et al., 2019) fall in the ranges for oceanic basalts with higher [K] (Tuller-Ross et al., 2019a): $-0.44 \pm 0.17\%$ for the MORB and $-0.41 \pm 0.16\%$ for the OIB. Our laboratory also reported data for other low-K samples ([K] $< 0.1\%$) such as chondrites (Bloom et al., 2020) and eclogites (Liu et al., 2020). No column fractionation or blank contamination have been observed for such low-K samples.

One low-K (58 $\mu\text{g/g}$) WR sample (spinel lherzolite 8530-5b-1) was processed and analyzed three times to assess repeatability of K isotope data (Table 1). One powder batch (8530-5-1b, 140 mg) was dissolved on a hot plate. Another batch (8530-5-1a; 598 mg) was dissolved in a Parr high-pressure digestion vessel and split in two aliquots that were chemically separated a few months apart. The $\delta^{41}\text{K}$ values in the duplicates (1.17‰, 1.12‰ and 1.06‰) reproduced within the uncertainties of individual measurements (Table 1).

4. Results

The samples are assembled below in five major groups (Table 1), based on their modal and chemical composition, and tectonic settings to clarify data presentation and discussion.

Group 1: fertile to moderately depleted lherzolites.

The nine Group 1 rocks are cpx-rich spinel and garnet-spinel lherzolites from Tariat and Vitim (Table 1, ES1, ES2). The content and ratios of major elements (e.g. Mg#, Al_2O_3 ; Table 1) in these samples approach those estimated for the BSE, but the concentrations of highly incompatible elements may be lower (ES2). Their PM-normalized WR rare earth element

(REE) patterns (Fig. 1a, b) are nearly flat or slightly depleted in the light REE (LREE) relative to the medium and heavy REE (Carlson and Ionov, 2019; Ionov et al., 2005a). The clinopyroxene in the same rocks has minor LREE depletions (Fig. 1a, b) as well as $^{87}\text{Sr}/^{86}\text{Sr}$, $^{143}\text{Nd}/^{144}\text{Nd}$ and $^{176}\text{Hf}/^{177}\text{Hf}$ ratios (ES3) that fall in the ranges for MORB (e.g. Hofmann, 2003; Ionov et al., 2005b). These features of the Group 1 rocks suggest that they are samples of mantle that is chemically and isotopically similar to the sources of modern MORB volcanism (Carlson and Ionov, 2019). The fertile lherzolites contain 7–90 $\mu\text{g/g}$ K with a $\delta^{41}\text{K}$ range from -1.09‰ to -0.49‰ (av. $-0.77 \pm 0.36\text{‰}$, 2sd; Table 1, Figs 2 and 3), and low K/La (Fig. 4).

Group 2: metasomatized, modally homogeneous intra-plate peridotites.

2a: Lightly metasomatized lherzolites with accessory amphibole \pm phlogopite. Such WR xenoliths usually have no or minor LREE enrichments (Fig. 1c), roughly proportional to modal amphibole, and low PM-normalized K/La ratios ($\text{K}/\text{La}_{\text{PM}} < 1$) (Fig. 4b). We report data for three WR samples as well as six amphiboles and a phlogopite separated from such xenoliths from the CAOBS, Germany and Australia (Ionov et al., 2005a; Ionov et al., 1992b; Ionov et al., 1997). These samples show a remarkably uniform $\delta^{41}\text{K}$ range from -0.77‰ to -0.37‰ (av. $-0.53 \pm 0.26\text{‰}$). Very similar $\delta^{41}\text{K}$ values were obtained on WR sample and on amphibole from xenolith 8603-2 (-0.73‰ and -0.77‰ , respectively) as well as on pure amphibole and a mixed amphibole-phlogopite fraction from sample 313-103 (-0.57‰ and -0.53‰) suggesting no inter-mineral K-isotope fractionation. The $\delta^{41}\text{K}$ values do not appear to be correlated with amphibole abundances, e.g. $\delta^{41}\text{K}$ for amphibole-rich ($>5\%$) peridotites 40-1 (-0.37‰) and Gn-1 (-0.53‰) are within the range for low-amphibole samples.

2b: Phlogopite-bearing cratonic harzburgites from the Udachnaya (ES2) and Obnazhennaya (Ionov et al., 2018) kimberlites, Siberia contain 1150–2750 $\mu\text{g/g}$ K with $\delta^{41}\text{K}$ from -1.05‰ to -0.35‰ , i.e. within the $\delta^{41}\text{K}$ range for the majority of off-craton peridotites (Fig. 3). The K concentrations in these highly refractory rocks are some of the highest in this study (Fig. 4a) while the K/La ratios are similar to those in the BSE indicating similar degrees of enrichments in K and in the LREE (Figs 1f and 4b). These xenoliths are much less affected by ingress of host kimberlite magma and post-eruption alteration than kimberlite-hosted xenoliths from other worldwide localities (e.g. Boyd and Nixon, 1978).

2c: Cryptically metasomatized off-craton harzburgites from Tariat (Carlson and Ionov, 2019; Press et al., 1986) contain no optically identifiable metasomatic minerals, but show strong continuous enrichments in LREE and MREE over HREE (Fig. 1e). These three samples have low [K] (88–135 $\mu\text{g/g}$), low K/La and very low $\delta^{41}\text{K}$ (-2.11% to -1.27%). The $\delta^{41}\text{K}$ values in these samples are lower than in any amph- and phl-bearing peridotites in Groups 2a and 2b (Figs 3 and 4).

2d: Metasomatized, feldspar-bearing lherzolite xenoliths from the CAO (Ionov et al., 1995) and the Pacific margin of Siberia (Ionov et al., 1999) in this study have 110–1900 $\mu\text{g/g}$ K (including some of the highest concentrations for off-craton WR peridotites, Fig. 4a) and $\delta^{41}\text{K}$ from -1.49% to -0.42% (av. $-1.00 \pm 0.68\%$, Fig. 3). The $\delta^{41}\text{K}$ in these six WR samples are generally lower and more scattered than for WR samples, amphibole and phlogopite of Group 2a xenoliths (Fig. 3). The WR REE patterns in Group 2d (Fig. 1d) range from REE-depleted to strongly LREE-enriched. As a result, the K/La ratios range broadly, with two samples having the highest K/La in this study (Fig. 4b).

2e: melt-pocket peridotites. Four xenoliths from Mongolia contain pockets of quenched glass with phenocrysts and vesicles formed in the mantle due to reaction of peridotites with metasomatic media shortly before their transport to the surface (Ionov et al., 1994). Sample 8530-5b records a transition from the initial stages of melting (8530-5b-1 with spongy cpx rims) to zones with spongy cpx and rare glass (8530-5b-2) and with mm-size glass pockets (8530-5b-3). The WR samples containing melt pockets have 170–330 $\mu\text{g/g}$ K, strong LREE-enrichments (Fig. 1h), low K/La and a broad $\delta^{41}\text{K}$ range from -2.15% to -0.61% (Figs 3 and 4).

Group 3: subduction-zone harzburgites.

Spinel harzburgites from the Avacha andesitic volcano (Ionov, 2010) define a separate group because of (a) tectonic setting in a subduction zone, and (b) modal and chemical compositions distinct from those of typical cratonic and off-craton intra-plate harzburgites. They are low in REE (Fig. 1e) and K (17–21 $\mu\text{g/g}$), have U-shaped REE patterns and higher K/La_{PM} (av. 1.5) than most other WR peridotites (apart from some phlogopite- and feldspar-rich xenoliths, Table 1) and show the highest $\delta^{41}\text{K}$ (0.40–0.62%; av. $0.51 \pm 0.30\%$) among WR xenoliths in this study.

Group 4: modally heterogeneous, metasomatized xenoliths

These rocks from Tariat in Mongolia (CAOB) formed either by interstitial percolation of fluids that created phlogopite-bearing domains in peridotites (Press et al., 1986) or by channelized intrusion of magmas and/or fluids to form cross-cutting pyroxenite and phlogopite-rich veins (Ionov et al., 1997; Ionov et al., 1998).

4a: lherzolites with phlogopite-rich domains. Spinel lherzolites Mo-70, 4230-16 and 4230-19 locally contain small, irregularly distributed, sub-parallel, prismatic phlogopite grains (Plate 4, ES1); their abundance ranges on cm-scale from zero to 1–3 wt.% (Ionov et al., 1997). These WR samples show moderate LREE enrichments (Fig. 1g) and contain 280 to 1080 ppm K with a $\delta^{41}\text{K}$ range of -0.31‰ to -0.06‰ (av. $-0.19 \pm 0.26\text{‰}$) (Figs 3 and 4). Phlogopite separated from a different portion of xenolith 4230-16 than that used to obtain its WR sample has a higher $\delta^{41}\text{K}$ (0.16‰ vs. -0.06‰ for the bulk rock).

4b: composite xenoliths (phlogopite-rich and pyroxenite veins in peridotites). Lherzolite Mo-71 (Plate 5, ES1) contains 474 $\mu\text{g/g}$ K (apparently hosted by rare accessory phl) and has the lowest $\delta^{41}\text{K}$ (-2.77‰) in this study. It hosts an irregular, 1–2 cm thick vein composed of coarse grains of phlogopite with $\delta^{41}\text{K}$ of -0.15‰ and cpx (Plate 5b, c, ES1). The difference in $\delta^{41}\text{K}$ between the vein phlogopite and the bulk host lherzolite sampled 2–5 cm from the vein (Plate 5a, ES1) is $\sim 2.6\text{‰}$.

Phlogopite-rich vein in lherzolite 4334-1 is modally zoned. Its center (4334-1u) is 5–10 mm thick and consists of medium-grained aggregate of phlogopite, cpx and apatite; the vein thins at the margins (4334-1g and 4334-1a) composed by intermittent subparallel phlogopite flakes. The $\delta^{41}\text{K}$ values for the phlogopite decrease from 0.57‰ in the center of the vein to -0.36‰ and -0.16‰ at the margins, with an overall center-rim difference of $0.7\text{--}0.9\text{‰}$.

Xenoliths 4230-15 and 4399-24 (Plate 6a,b; ES1) represent another type of composite mantle samples: peridotites cross-cut by ~ 2 cm thick pyroxenite veins (Ionov et al., 1998). Lherzolite 4230-15Lh is low in K (52 $\mu\text{g/g}$) and has a low $\delta^{41}\text{K}$ (-1.38‰). By contrast, spinel websterite vein 4230-15v that contains accessory phlogopite, has much more K (2327 $\mu\text{g/g}$) and higher $\delta^{41}\text{K}$ (-0.33‰ vs. -1.38‰ in the host lherzolite). The host-vein relations in this xenolith are similar to those in sample Mo-71. Phlogopite-bearing lherzolite 4399-24Lh contains more K than garnet-orthopyroxenite vein 4399-24v (1220 vs. 340 $\mu\text{g/g}$) and has

lower $\delta^{41}\text{K}$ than the vein (-0.35‰ vs. -0.17‰). Overall, the pyroxenite veins in both composite samples have lower $\delta^{41}\text{K}$ than the peridotite hosts while the K concentrations are either lower or higher.

Group 5: pyroxenites and mantle-derived volcanic rocks.

5a: discrete pyroxenite xenoliths formed in the mantle from mafic magmas (Frey and Prinz, 1978). Black pyroxenites 8530-81 and 4399-7 have low Mg# (≤ 0.8) and $>1\%$ phlogopite suggesting formation from more evolved and more volatile-rich mafic liquids than green garnet pyroxenite 4230-18. These three WR samples from Tariat have 383–13039 $\mu\text{g/g}$ K and $\delta^{41}\text{K}$ from -0.72‰ to -0.29‰ (av. $-0.51 \pm 0.42\text{‰}$); the $\delta^{41}\text{K}$ value for pyroxenite 8530-81 is identical to that for phlogopite separated from this sample. A single lower crustal granulite in this study from the same site has a $\delta^{41}\text{K}$ of -0.53‰ , i.e. within the range for the pyroxenites.

5b: volcanic rocks hosting mantle xenoliths were analyzed to (a) evaluate potential contamination of the WR xenoliths by host magma, and (b) compare $\delta^{41}\text{K}$ for different continental intra-plate mafic magmas with subduction zone andesites and their crystallization products. Fresh kimberlite K-27-04 from the Udachnaya pipe on the Siberian craton (Kamenetsky et al., 2012) has $\delta^{41}\text{K} = -0.40 \pm 0.07\text{‰}$. Three samples (vesicular lava, glass fragment and phlogopite megacryst) from the Shavaryn-Tsaram volcanic breccia in Tariat (Press et al., 1986) show a $\delta^{41}\text{K}$ range of -0.47‰ to -0.27‰ (av. $-0.40 \pm 0.18\text{‰}$). Three samples (amph-cpx-olivine cumulates and separated amphibole) crystallized from parental magmas of Avacha andesites hosting Group 3 xenoliths have a narrow $\delta^{41}\text{K}$ range from -0.44‰ to -0.53‰ (av. $-0.49 \pm 0.10\text{‰}$). Altogether the $\delta^{41}\text{K}$ in the seven samples define a range of -0.27‰ to -0.53‰ with an average of $-0.45 \pm 0.08\text{‰}$.

5. Discussion

5.1 Potassium in fertile and melt-depleted mantle peridotites

Highly incompatible elements, including K, in upper mantle peridotites reside not so much in the crystal lattice of major minerals (olivine, pyroxenes, garnet) as in intra-granular inclusions and minute inter-granular (grain-boundary) components, as shown by natural and experimental studies, and thermodynamic modeling (e.g. Hiraga and Kohlstedt, 2009). The

grain-boundary materials in pristine or residual mantle form due to equilibrium partitioning of elements with low distribution coefficients (D) in its major minerals (Hiraga et al., 2004) and were found in metasomatized rocks as well (e.g. Bedini and Bodinier, 1999).

Mineral/melt D values for K in olivine and pyroxenes are ≤ 0.01 (GERM database: <https://earthref.org/KDD/e:19/>). Extraction of 3% of partial melt from primitive mantle (258 $\mu\text{g/g}$; Hofmann (1988)) may remove $\geq 75\%$ of K by batch melting and $\geq 95\%$ by equilibrium melting leaving 65–13 $\mu\text{g/g}$ K in residues, similar to the [K] range in fertile lherzolites in this study (90–7 $\mu\text{g/g}$; Table 1). The PM-normalized element patterns of these rocks (Fig. 1a, b), however, show very strong K depletions relative to La, which has similar peridotite/melt D values. Decoupling of the REE and K abundances is also seen in some metasomatized peridotites (Fig. 1d, e and h). This could be explained either by much lower peridotite/melt D values for K relative to the LREE than those in the literature, or by K redistribution or removal via late-stage fluid circulation on cooling of melting residues due to high mobility of K in fluids. The latter option may be more plausible because low K/La ratios are mainly observed in samples that contain no discernible K-rich phases (phlogopite, feldspar).

5.2 K-isotope composition of the BSE and MORB-source mantle

Modern Earth reservoirs were formed by fractionation of the BSE (PM). Removal of small amounts (totaling $\sim 1.5\%$) of partial melts from the BSE built up a proto-crust and depleted the residues (depleted MORB mantle, DMM) in the incompatible elements that are enriched in the crust (Hofmann, 1988). Recycling of crustal materials to the DMM created hybrid OIB-type asthenospheric regions (e.g. Hofmann and White, 1982). In the absence of evidence that any BSE portions still exist, the abundances and isotope compositions of the highly incompatible elements in the BSE cannot be evaluated directly, but have to be constrained from data on appropriate samples from the modern reservoirs.

Fertile lherzolites from Tariat and Vitim are samples of MORB-source asthenosphere added to the CLM (Carlson and Ionov, 2019; Ionov et al., 2005a). The content and stable isotope compositions of compatible and slightly incompatible elements in mantle rocks that experienced the lowest melt extraction degrees are basically the same as in the BSE because they are little affected by melting (Carlson and Ionov, 2019; Salters and Stracke, 2004; Teng

et al., 2017). This is why some of the Tariat and Vitim xenoliths were previously used to constrain the stable isotope ratios of such elements (hosted by at least one mineral phase in the peridotites: olivine, pyroxenes, garnet and spinel) in the BSE: Ca (Kang et al., 2017), Cr (Xia et al., 2017), Fe (Weyer and Ionov, 2007), Li, Mg (Pogge von Strandmann et al., 2011), Zn (Doucet et al., 2016), Ni, V (see ES3 for more references).

By contrast, the K content in such rocks is an order of magnitude lower than in BSE estimates because highly incompatible elements are largely extracted from solids even at very low melting degrees (e.g. Hofmann, 1988), and none of the common minerals in the uppermost mantle are significant K hosts. It is not clear if the potential removal of ~90% of the initial K inventory in the BSE has modified K isotopic composition in the residual mantle, but possibly not a lot, because data on differentiated magmatic series show that K isotopes are not affected by magmatic fractionation, i.e. partial melting and fractional crystallization (Hu et al., 2021b; Tuller-Ross et al., 2019b), consistent with unresolvable equilibrium isotope fractionation at high temperatures (Li et al., 2019b; Zeng et al., 2019). Besides, much K in non-metasomatized peridotites is hosted by inter-granular materials, hence its loss does not involve K transfer from one phase to another. Recent studies (Tuller-Ross et al., 2019a) found no significant differences in $\delta^{41}\text{K}$ between oceanic basalts from different regions generated by different melting degrees which implies no detectable K isotope fractionation during partial melting. By contrast to basaltic magmas that deliver averaged estimates for their source compositions, the xenolith data may indicate moderate sample-to-sample $\delta^{41}\text{K}$ variations in the CLM.

The best $\delta^{41}\text{K}$ estimate for fertile CLM (av. $-0.65 \pm 0.30\text{‰}$) is obtained here from data on four Tariat lherzolites (Mo53389, S1, S54, MOG-5) with the major oxide (av. 4.45 wt.% Al_2O_3 , Mg# = 0.893) and REE (Fig. 1a) content nearest to PM estimates (Palme and O'Neill, 2003). It is slightly lower, but within uncertainty of the average $\delta^{41}\text{K}$ for oceanic basalts ($-0.43 \pm 0.17\text{‰}$) after Tuller-Ross et al. (2019a) (Figs. 2 and 3). The high uncertainty of this estimate, together with broad [K] range in these samples (7 to 57 $\mu\text{g/g}$), may be due to post-melting K re-distribution by low-volume fluids that affect inter-granular components hosting K in these melting residues (e.g. Bedini and Bodinier, 1999), but do not modify

conventional metasomatism indices like the patterns of REE that are mainly hosted by clinopyroxene.

Several lines of evidence suggest that the $\delta^{41}\text{K}$ values in these xenoliths have not been affected by hypothetical contamination by host magmas with [K] over 3 orders of magnitude higher ($\sim 3 \cdot 10^4 \mu\text{g/g}$; Table 1). First, sampling procedures and thin section (Plates 1–3, ES1) examination rule out the presence of basalt in the WR samples. Second, the K/La and K/Rb ratios in these samples (31–124 and 153–219, respectively; Table 1, ES2) are much lower than in host lava Mo-23 (K/La = 585, K/Rb = 721) suggesting that their inventories of the highly incompatible elements are not controlled by magma infiltration. The $\delta^{41}\text{K}$ average for these xenoliths ($-0.65 \pm 0.30\%$) is not very different from $\delta^{41}\text{K}$ in the host basalt (-0.47%) implying that minor basalt additions may not significantly affect their $\delta^{41}\text{K}$. Finally, phlogopite-free Tariat xenoliths (including harzburgites) do not plot on model mixing lines of low-K ($7\text{--}37 \mu\text{g/g}$) peridotites with host basalt Mo-23 on plots of [K] vs. K/La and $\delta^{41}\text{K}$.

Five other spinel and garnet-spinel lherzolites from Tariat and Vitim (Ionov et al., 2005a) are less fertile (lower Al_2O_3 , higher Mg#), hence underwent more melt extraction, but show LREE-depleted patterns (Fig. 1a,b), i.e. no evidence for melt metasomatism. Their $\delta^{41}\text{K}$ range (-1.09 to -0.71% , av. $-0.86 \pm 0.32\%$) is lower than for the more fertile lherzolites. These data cannot be interpreted as indicating that $\delta^{41}\text{K}$ in residual mantle decreases at higher melting degrees because, as discussed above in this section, K isotope fractionation during partial melting is insignificant. Furthermore, the Vitim xenoliths hosted by 16 My old tuffs have minor secondary alteration and fine-grained materials (kelyphite) at rims of garnet grains (e.g. Ionov et al., 2005b); their average $[\text{K}_{\text{WR}}]$ is twice as high as for the generally unaltered Tariat xenoliths ($64 \pm 62 \mu\text{g/g}$ vs. $29 \pm 36 \mu\text{g/g}$). Studies of crustal rocks show that surface alteration may decrease $\delta^{41}\text{K}$ values (Chen et al., 2020; Teng et al., 2020).

The estimate for non-metasomatized fertile CLM lherzolites (residues of low-degree melt extraction) has a high uncertainty as the samples are few and the provenance of K at mainly low, but variable, K content may be ambiguous, e.g. because they may be prone to cryptic metasomatism. An alternative to obtain an estimate for “normal off-craton CLM” is to combine the data for the most fertile Group 1 Tariat lherzolites with those for Group 2a lightly metasomatized lherzolites for three major reasons. (a) Such amphibole-bearing

lherzolites are common in the mantle, and (b) contain enough K not to be biased by minor additions of K before, during and after eruption. (c) They show very consistent $\delta^{41}\text{K}$ values (av. $-0.53 \pm 0.26\text{‰}$) suggesting no significant isotope fractionation during low-degree, bulk metasomatism, likely via additions of fluids escaped from sub-lithospheric mantle. The average for these 14 samples ($-0.57 \pm 0.28\text{‰}$) is closer to averages for oceanic basalts.

5.3 Metasomatism-linked K isotope variations in the CLM

5.3.1 Metasomatized lherzolites (Group 2a, d)

The most common metasomatic rocks in off-craton CLM appear to be Group 2a lherzolites with accessory amphibole \pm minor phlogopite (Best, 1974; Dawson and Smith, 1982) and minor to moderate K-enrichments relative to non-metasomatized Group 1 rocks (Fig. 1c). The mean $\delta^{41}\text{K}$ ($-0.53 \pm 0.26\text{‰}$) of these samples overlaps averages for non-metasomatized lherzolites ($-0.65 \pm 0.30\text{‰}$) and oceanic basalts ($-0.43 \pm 0.17\text{‰}$) (Tuller-Ross et al., 2019a). These generally fertile rocks probably experienced addition of small amounts of low-K metasomatic fluids from upwelling asthenosphere via simple mixing (Frey and Green, 1974; Stosch and Seck, 1980) without significant isotope fractionation.

By contrast, the generally higher $[\text{K}_{\text{WR}}]$ (300–1900 $\mu\text{g/g}$) and LREE-enrichments in Group 2d feldspar-bearing lherzolites indicate a stronger metasomatism that locally yields lower $\delta^{41}\text{K}$ (-1.49 to -0.42‰). Five out of six samples in this group have $\delta^{41}\text{K}$ of -1.49 to -0.93‰ (av. $-1.11 \pm 0.43\text{‰}$), much lower than in oceanic basalts (hence in their sources), indicating that low $\delta^{41}\text{K}$ could be typical of this type of metasomatism. One way to explain the ubiquitously low $\delta^{41}\text{K}$ values in this group could be an origin from peculiar metasomatic media. Some subducted sediments or dehydrated altered oceanic crust (e.g. eclogite, Fig. 3) were reported to have very low $\delta^{41}\text{K}$ ascribed to continental weathering and submarine diagenetic alteration (Liu et al., 2020; Sun et al., 2020). In particular, marine sediments have a broad $\delta^{41}\text{K}$ range (-1.3 to -0.02‰ ; Hu et al. (2020b)) but generally lighter K isotopic compositions than oceanic basalts. The addition of subducted sediments to mantle sources of metasomatic media would produce a shift to lower $\delta^{41}\text{K}$ values, though it is not clear if this shift could be sufficient to explain the lowest $\delta^{41}\text{K}$ values in our Group 2d xenoliths.

While this kind of interpretation may fit the samples from Barhatny near the Pacific coast of Siberia (Rudnick and Ionov, 2007), it is less likely for similar xenoliths from Hamar-Daban in the center of Asia with no apparent links to modern or recent subduction zones (Ionov et al., 1999; Ionov et al., 1995). Yet, low- $\delta^{41}\text{K}$ fluids could stem from eclogites from an ancient subduction zone incorporated into sub-lithospheric mantle (see *section 5.3.3*).

Another important clue to the origin of the feldspar lherzolites, and possibly their $\delta^{41}\text{K}$ values, is the absence of amphibole and phlogopite in these samples suggesting that parental metasomatic media were low in water, i.e. either came from ‘dry’, carbonate-rich sources (Delpech et al., 2004) or, alternatively, lost water on the way due to precipitation of hydrous phases in or next to their feeders (Ionov et al., 2006).

An alternative way to explain low $\delta^{41}\text{K}$ in mantle peridotites could be kinetic K-isotope fractionation during fluid-rock reactions. Morgan et al. (2018) found largely uniform $\delta^{41}\text{K}$ values for 30 igneous and metamorphic crustal rocks and minerals, but greater $\delta^{41}\text{K}$ variability in some high-temperature suites affected by fluids, notably -0.11 to -1.36‰ in pegmatites (Fig. 3) with lower $\delta^{41}\text{K}$ values in later crystallizing assemblages. Morgan et al. (2018) attributed the variations to K-isotope fractionation by chemical or thermal (Soret) diffusion as suggested from previous studies in pegmatites and their country rocks using Li isotopes and experimental observations (Richter et al., 2009; Teng et al., 2007) as well as laboratory measurements of Li diffusion coefficients in minerals (Richter et al., 2014a). It may be relevant that Rudnick and Ionov (2007) reported anomalously low $\delta^7\text{Li}$ in Group 2d xenolith 9513-8. A problem with such an interpretation however is that fractionation ought to produce both heavier and lighter isotope values from a given source whereas $\delta^{41}\text{K}$ in the Group 2d xenoliths are generally lower than BSE estimates. This implies that the putative fractionation ought to take place in the sources and feeders of metasomatic media rather than in the CLM domain where the xenoliths come from. Discussion of kinetic K isotope fractionation is given in *section 5.3.4* on composite xenoliths with broad $\delta^{41}\text{K}$ ranges.

5.3.2 Harzburgites and melt-pocket peridotites (Group 2b, c, e)

Harzburgites and other refractory (low-Al, high-Mg#) peridotites produced by extensive melt extraction were initially depleted in incompatible elements, but then overprinted by metasomatism (e.g. Frey and Green, 1974), probably because of high permeability of olivine-rich rocks to metasomatic media (Nakano and Fujii, 1989; Toramaru and Fujii, 1986). They cannot be used to assess K-isotope composition of residual, melt-depleted mantle.

The olivine-rich, low-cpx peridotites in this study (Group 2b, c, e) have the highest LREE/HREE ratios (Fig. 1e, f, h) suggesting important metasomatic enrichments, but the $[K_{WR}]$ and $\delta^{41}K$ in different rock types range broadly. We attribute these differences to modal compositions and types of metasomatism. Phlogopite-bearing harzburgites from the Siberian craton (Group 2b) have the highest $[K_{WR}]$ (1150-2750 $\mu\text{g/g}$; Fig. 4) and show no evidence for isotope fractionation or unusual metasomatic sources because their $\delta^{41}K$ values (-1.05‰ to -0.35‰ ; av. $-0.69 \pm 0.70\text{‰}$) are similar to those for fertile and lightly metasomatized mantle (Groups 1 and 2a; Fig. 3) and thus may fall in the $\delta^{41}K$ range of common mantle metasomatic media. The $\delta^{41}K$ in two xenoliths from the Obnazhennaya pipe that also contain metasomatic carbonates (Ionov et al., 2018) are similar to $\delta^{41}K$ for carbonate-free xenoliths from the Udachnaya pipe suggesting that ‘carbonatite’ mantle metasomatism (e.g. Green and Wallace, 1988) may not have a specific K-isotope signature, as is also the case for some other stable isotope systems like Ca (Ionov et al., 2019; Sun et al., 2021).

The cryptically metasomatized and melt-pocket peridotites have a broader $\delta^{41}K$ range (-0.41 to -2.15‰ ; Fig. 3), lower average $\delta^{41}K$ (-1.56 and -1.06‰) and low $[K_{WR}]$ (17–160 $\mu\text{g/g}$) and K/La (Fig. 4). Peculiar sources of metasomatic media are questionable for such rocks that are ubiquitous in the CLM, and a likely alternative is kinetic isotope fractionation due to faster diffusion for ^{39}K than for ^{41}K in metasomatic media. Numerical modeling and studies of veined mantle show that during percolation of metasomatic media from feeders to host mantle, phlogopite and amphibole are precipitated close to the source while residual fluids at the percolation front become progressively depleted in water and K trapped in the hydrous phases (Bodinier et al., 1990; Menzies et al., 1985). We speculate that low-water liquids at the percolation front could be enriched in the light ^{39}K . Cryptically metasomatized peridotites with low $\delta^{41}K$ may thus be located at greater distances from fluid sources than phl- and amph-bearing rocks in metasomatic aureoles (as discussed in *section 5.3.4*).

5.3.3 Subduction zone mantle (Group 3)

Andesite-hosted harzburgite xenoliths from Kamchatka document a particular case of mantle metasomatism above an oceanic subduction zone. Their protolith formed by high degrees of melt extraction (Bénard et al., 2021; Ionov, 2010), which removed essentially all K from its DMM source. Nearly all K in the Kamchatka harzburgites must have been brought in by metasomatic media and is hosted by the late-stage, interstitial amphibole and glass inclusions (Ionov et al., 2011). Metasomatic melts trapped in minerals of these rocks are more oxidized than normal mantle, which indicates contributions of agents formed by dehydration of serpentinised slab (Bénard et al., 2018).

The Kamchatka harzburgites have higher $\delta^{41}\text{K}$ than oceanic mantle (i.e. the MORB and OIB sources) and are the only group of rocks in this study with positive $\delta^{41}\text{K}$ (Figs. 2 and 3). Equilibrium isotope fractionation during metasomatism could not enrich the rocks in heavy K because peridotite-melt isotopic fractionation at magmatic temperatures is negligible (e.g. Hu et al., 2021b; Tuller-Ross et al., 2019b). Furthermore, this study found no positive $\delta^{41}\text{K}$ values in amphibole-bearing peridotites from intra-plate CLM (Group 2a). Thus, it appears that the $\delta^{41}\text{K}$ values in the Kamchatka xenoliths are inherited from subduction-related fluids.

Several recent studies support this inference. Hu et al. (2021a) reported arc lavas with variably high $\delta^{41}\text{K}$ (-0.28 to 0.01%) likely caused by the addition of isotopically heavy K-bearing fluids derived from slab dehydration and argued that a substantial fraction of K in arc magmas is inherited from subducted crust. Liu et al. (2020) found very low $\delta^{41}\text{K}$ (-1.64 to -0.24%) in eclogites from Tibet (Fig. 3) compared to their MORB sources ($-0.43 \pm 0.17\%$), and a positive correlation between $\delta^{41}\text{K}$ and K/Nb ratios. They attributed the low $\delta^{41}\text{K}$ in the eclogites to isotope fractionation via slab dehydration during subduction-related prograde metamorphism that produced low- $\delta^{41}\text{K}$ eclogites and complementary high- $\delta^{41}\text{K}$ slab-derived fluids. Rayleigh fractionation modeling (Liu et al., 2020) yielded a $\delta^{41}\text{K}$ range of 0.23 to 1.04% for such fluids which overlap the $\delta^{41}\text{K}$ of the subduction zone harzburgites in this study (0.40 to 0.62%). In the same vein, Marschall et al. (2007) inferred large-scale kinetic fractionation of Li isotopes (-22% to $>+6\%$) during diffusive influx of Li in orogenic metamorphic rocks during subduction and exhumation.

Liu et al. (2021) inferred that slab-derived fluids contributed heavy K isotopic signatures to the mantle source of ultrapotassic rocks in central China that show $\delta^{41}\text{K}$ ranging from -0.57‰ to -0.06‰ as well as positive correlations with K/Th, Ba/Th and Ba/Rb ratios, which can be modelled by the mixing of MORB-like mantle with <10% fluids derived from the subducting slabs. Likewise, Sun et al. (2020) reported a larger $\delta^{41}\text{K}$ range (-0.81‰ to -0.15‰) for basaltic lavas from NE China than for unaltered oceanic basalts ($-0.43 \pm 0.03\text{‰}$) and linked the differences to the presence of recycled oceanic crust and sediments in their mantle sources, enriched in heavier and lighter K isotopes, respectively.

To sum up, the high- $\delta^{41}\text{K}$ fluids released into the mantle wedge could be responsible for the high $\delta^{41}\text{K}$ in the Kamchatka harzburgites. Such fluids were added to melting residues as they were incorporated into the lithospheric mantle of the wedge (e.g. Wang et al., 2017). Overall, the literature data suggest that subducted oceanic slabs may contain two types of materials that can be sources of fluids with different K-isotope signatures at different stages and conditions of subduction. Slab dehydration and prograde metamorphism produce high- $\delta^{41}\text{K}$ fluids that affect the mantle wedge. The complementary low- $\delta^{41}\text{K}$ eclogites are stored in the asthenosphere and could eventually be sources of low- $\delta^{41}\text{K}$ metasomatic media similar to those responsible for K isotope signatures in Group 2b-e xenoliths in this study (*sections 5.3.1 and 5.3.2*).

The harzburgite xenoliths and associated pyroxenite veins from Kamchatka display BSE-like values (ES3) of $\delta^{26}\text{Mg}$ (-0.30 to -0.21‰) and $\delta^{56}\text{Fe}$ (0.00 to -0.06‰) (Hu et al., 2020a; Weyer and Ionov, 2007). The lack of a clear slab-derived $\delta^{26}\text{Mg}$ and $\delta^{56}\text{Fe}$ signatures in these sub-arc xenoliths is due to their high Mg and Fe content and low fluid/rock mass ratios during flux melting and metasomatism, i.e. the metasomatic Mg and Fe ingress is too small to affect $\delta^{26}\text{Mg}$ and $\delta^{56}\text{Fe}$ in the host mantle (Hu et al., 2020a). The opposite is the case for stable isotopes of highly incompatible trace elements like K whose metasomatic contributions are dominant relative to those in generally K-depleted host mantle.

5.3.4 Heterogeneous mantle

Modally heterogeneous phlogopite-bearing lherzolites and veined xenoliths (Group 4) show the greatest $\delta^{41}\text{K}$ range, from -2.77 to 0.57‰ that overlaps the $\delta^{41}\text{K}$ ranges for the

most common CLM rocks (fertile and lightly metasomatized lherzolites), but is much wider. The fact that large $\delta^{41}\text{K}$ variations in this group are observed within a few cm in single xenoliths (up to 2.6‰; Fig. 5) makes an origin from batches of metasomatic media with very different K isotope compositions highly unlikely. Rather, the data lead us to examine the possibility that the highly contrasted $\delta^{41}\text{K}$ ranges in these samples may be due to extreme local (cm-scale) kinetic isotope fractionation of initially isotopically homogeneous liquids or fluids (Richter et al., 2014b), e.g. those with BSE-like initial $\delta^{41}\text{K}$.

The most striking case of local K-isotope disequilibrium is recorded in composite Tariat xenolith Mo-71 (Plate 5, ES1) between coarse phlogopite vein ($\delta^{41}\text{K} -0.15\text{‰}$) and the host lherzolite ~2–5 cm away containing 474 $\mu\text{g/g}$ K with $\delta^{41}\text{K} -2.77\text{‰}$ (Figs 4–5). Potassium in the host lherzolite must have infiltrated from the vein since the great majority of lherzolite xenoliths in the Tariat suite have much lower [K] (Table 1) and no phlogopite (Carlson and Ionov, 2019). We speculate that K-bearing fluid that escaped to the host from the vein was enriched in ^{39}K relative to ^{41}K due to faster diffusion of the lighter isotope leaving behind ^{41}K -enriched fluid batches that formed vein phlogopite. Mass balance factors suggest that the fractionation effects for the host lherzolite (that initially had very little K) should be much greater than for the phlogopite vein. Thus, fractionation of a source fluid with $\delta^{41}\text{K}$ of -0.4‰ , like in the DMM and OIB source regions (Tuller-Ross et al., 2019a), could possibly yield a vein with $\delta^{41}\text{K}$ of -0.15‰ and a host lherzolite with -2.77‰ .

Relative diffusion rates for solute isotopes are usually expressed using the ratio of their diffusion coefficients (D_2/D_1) as an inverse power-law function of the ratio of their masses, m_2 and m_1 (Richter et al., 2009; Watkins et al., 2017): $(D_2/D_1) = (m_1/m_2)^\beta$ where β is a dimensionless empirical parameter that allows for direct comparison between pairs of isotopes that have different fractional mass differences (e.g. the mass difference for $^7\text{Li}/^6\text{Li}$ is ~14% versus ~5% for $^{41}\text{K}/^{39}\text{K}$). Laboratory experiments and natural rocks have shown very large isotopic fractionation at high temperatures for lithium, another alkali metal, due to the significantly faster (up to 3%) diffusivity of ^6Li relative to ^7Li in melts, minerals and rocks (Pogge von Strandmann et al., 2008; Richter et al., 2009; Rudnick and Ionov, 2007).

So far the experiments have only examined the thermal (Soret) isotopic fractionation of K in a basalt melt (Richter et al., 2014b), but we are not aware of experimental data for K

diffusion caused by chemical gradients at mantle conditions. Apart from the lack of diffusion coefficients, modeling K outflow from a conduit filled with a K-rich silicate melt or fluid to host mantle faces other hurdles. Experiments usually constrain diffusion parameters for homogeneous melts or minerals whereas K likely migrates from veins via fluid percolation or fluid-assisted grain-boundary diffusion, and is ultimately hosted at grain margins and/or in intermittent accessory phases (phl, amph, feldspar). If such data were known (diffusion coefficients, width of fluid channels, fluid connectivity, role of K-rich microphases), these processes could be quantitatively tested. Another currently missing parameter is spatial geochemical data on samples collected at various distances from the vein to see if they show a diffusion profile or suggest other complex processes. This necessitates larger xenoliths than in this study because coarse-grained mantle rocks with irregular mineral distribution (see ES1) require much material (>3 cm) for representative sampling.

Some previous work on massif peridotites and mantle xenoliths including samples from this study (Lundstrom et al., 2005; Pogge von Strandmann et al., 2011; Weyer and Ionov, 2007) used numerical modeling of intra-grain or mineral-melt diffusion for Li, Mg and Fe isotopes in olivine and/or pyroxenes to explain heterogeneous isotope distribution in minerals and bulk xenoliths. Such modeling, however, cannot be directly applied to examine the transport of potassium (and other highly incompatible elements) because major mantle minerals contain essentially no K, which thus cannot migrate via solid-state diffusion.

We report here data on four veined xenoliths, and in all the cases the veins have heavier K isotopes than the hosts (Fig. 5); the probability of this to be occasional is very low. We posit that fluids migrating from feeders to host mantle could be fractionated and enriched in ^{39}K relative to ^{41}K near percolation front due to faster diffusion of the lighter isotope. Such an explanation is qualitatively consistent with chemical diffusion experiments and natural observations for stable isotopes of Li, Mg, Ca, Fe, Cr and other elements in mantle samples (Kang et al., 2020; Watkins et al., 2017; Wu et al., 2018) including those from the same xenolith sites as in this study (e.g. Kang et al., 2017; Pogge von Strandmann et al., 2011).

The phlogopite (4334-1u) with the highest $\delta^{41}\text{K}$ in Group 4 comes from the center of a vein filling a former feeder of K-rich fluids (Fig. 5). The fluids spread laterally by inter-granular diffusion and percolation to form accessory phlogopite in the host mantle. We

posit that phlogopite formed near the metasomatic front far from the feeder (samples 4334-1a and -1g at veins margins) was enriched in ^{39}K , which diffuses faster than ^{41}K , i.e. had lower $\delta^{41}\text{K}$ (-0.36 and -0.16%) than the phlogopite deposited in the feeder when fluid inflow stopped (0.57%). Other samples in this group may represent materials located at different distances from their respective sources of K-rich fluids as well.

Similar processes took place during the formation of pyroxenite veins in two composite xenoliths from Tariat, 4230-15 and 4399-24. The veins are cumulates from magma that flowed in fractures in the host mantle (Ionov et al., 1998; Witt-Eickschen and Kramm, 1998); the magma feeders could have been larger than the veins (Xia et al., 2017). Potassium diffused from the magma to the host mantle producing enrichments in ^{39}K near the diffusion (or fluid percolation) front, whereas the remaining melt was depleted in ^{39}K relative to ^{41}K . This explains why both xenoliths show lower $\delta^{41}\text{K}$ in the host lherzolites than in the veins (Fig. 5). The [K] in the veins and hosts depends on the presence of phlogopite, the only K-rich mineral in the xenoliths, which forms from fluids in rocks with appropriate modal and major oxide compositions. Lherzolite 4399-24Lh contains phlogopite at the contact with the vein which explains higher $[\text{K}_{\text{WR}}]$ in the host; this sample has the smallest vein-host $\delta^{41}\text{K}$ contrast (-0.36 and -0.16% ; Fig. 5).

These two samples were previously analyzed for Cr (Xia et al., 2017) and Ca isotopes (Kang et al., 2019). The $\delta^{53}\text{Cr}$ values are lower in the veins than in the host peridotites. The vein-host $\delta^{53}\text{Cr}$ relations were explained by kinetic isotope fractionation as well, but the difference is that the host peridotites had higher [Cr] than the magma such that Cr diffused from the peridotites to the magma in feeders. The magma was thus enriched in the lighter ^{52}Cr isotope and crystallized vein materials with lower $\delta^{53}\text{Cr}$. By contrast, the $\delta^{44/40}\text{Ca}$ values of the veins and the hosts are similar because both the host lherzolites, that contain 15–20% cpx with ~20 wt.% CaO, and the magma had roughly similar Ca content. There was no preferential transport of Ca either to or from the feeders, and the pyroxenes both in the host peridotites and the vein may have attained Ca-isotope equilibrium.

5.4 $\delta^{41}\text{K}$ in mantle vs. crustal materials

Figure 3 shows a summary of published K isotopic data on mantle and crustal materials. A comprehensive study of typical rocks in the upper continental crust (diorite, granodiorite, granite, loess, shale, graywacke, pelite and tillite) found a moderately heterogeneous $\delta^{41}\text{K}$ range from -0.68 to -0.12‰ with a weighted average of $-0.44 \pm 0.05\text{‰}$ ($n = 88$) (Huang et al., 2020). This range and average are indistinguishable from the current data on oceanic basalts (Tuller-Ross et al., 2019a; Wang and Jacobsen, 2016), in line with the absence of K-isotope fractionation during magmatic differentiation (Hu et al., 2021b; Tuller-Ross et al., 2019b).

The $\delta^{41}\text{K}$ values in xenolith-bearing volcanic materials (-0.53 to -0.27‰ , av. $-0.44 \pm 0.17\text{‰}$) and discrete pyroxenites (-0.72 to -0.29‰ , av. $-0.51 \pm 0.17\text{‰}$) in this study fall in the range for the continental crust and yield a similar overall average ($-0.47 \pm 0.24\text{‰}$) (Fig. 2). A single lower crustal granulite xenolith in this study falls in the middle of this range (Table 1). The four analyses for the cratonic and intra-plate volcanic rocks fall in the $\delta^{41}\text{K}$ range ($-0.43 \pm 0.17\text{‰}$) reported for oceanic basalts (Tuller-Ross et al., 2019a; Wang and Jacobsen, 2016).

Modern low-temperature altered oceanic crust (AOC) and fossil oceanic lithosphere (ophiolites) show similar $\delta^{41}\text{K}$ ranges, -0.88 to 0.04‰ and -1.07 to 0.19‰ , respectively (e.g. Parendo et al., 2017; Santiago Ramos et al., 2020), i.e. are generally isotopically lighter than seawater ($0.14 \pm 0.02\text{‰}$) (Hille et al., 2019; Wang et al., 2020). The AOC is a major sink for K from seawater, and the $\delta^{41}\text{K}$ range of modern and ancient AOC can be explained by K isotopic fractionation between seawater and low-temperature alteration clay minerals.

This study reveals a much broader $\delta^{41}\text{K}$ range (-2.77 to 0.62‰) in the lithospheric mantle than in the exposed crust (Figs 2 and 3). However, as noted in *Section 5.2*, the most common CLM rocks (fertile and lightly metasomatized lherzolites) define a narrower range of -1.09 to -0.37‰ , with an average ($-0.57 \pm 0.28\text{‰}$) close to averages for oceanic basalts and continental crust. Moreover, an average for all CLM xenoliths in this study ($-0.7 \pm 0.9\text{‰}$) falls within the range of the oceanic and upper continental crust.

The reason for the broad overall $\delta^{41}\text{K}$ range in this study is that it includes samples from different tectonic settings (craton, mobile belts, subduction zone) as well as rocks with a broad range of modal and chemical compositions, in particular those affected by mantle

metasomatism. Furthermore, some of the samples explore mantle heterogeneities on a cm scale, including modally heterogeneous and veined xenoliths affected by small-scale non-equilibrium isotope fractionation. This contrasts with recent studies on crustal materials that seek to constrain K isotopic variations in common crustal rocks (e.g. Huang et al., 2020). Yet, a broader $\delta^{41}\text{K}$ range (-1.07 to $+0.04\text{‰}$) was reported for weathered and hydrothermally altered continental rocks and ophiolites (Chen et al., 2020; Santiago Ramos et al., 2020; Teng et al., 2020).

As noted in *Section 5.2*, no single modern Earth reservoir can be *a priori* considered as representative of the K isotope composition of the BSE because (a) all of them are BSE fractionation products and (b) the concentrations of the highly incompatible K can be strongly fractionated by even small degrees of melt extraction, migration and crystallization. This is why, strictly speaking, estimating the $\delta^{41}\text{K}$ for the BSE may require adding up mass-weighted data on these reservoirs. This study provides data on yet unexplored pieces of this global “jigsaw puzzle”, the CLM and mantle wedge lithosphere. The CLM estimate ($-0.57 \pm 0.28\text{‰}$) confirms that the major Earth’s reservoirs appear to have similar bulk $\delta^{41}\text{K}$ values: $-0.44 \pm 0.17\text{‰}$ and $-0.41 \pm 0.16\text{‰}$ for the DMM and OIB source regions (Tuller-Ross et al., 2019a), and $-0.44 \pm 0.05\text{‰}$ for the continental crust (Huang et al., 2020). This similarity appears to be due to negligible K isotopic fractionation during their formation by melting and magmatic differentiation. The only exception appears to be modern (and possibly fossil) subduction zones where K isotopes may be fractionated via fluid-related equilibrium and kinetic processes, and thus could be priorities for further work. Little data is available on the behavior of potassium in deep mantle though experimental work suggests that it may be compatible in the deep mantle (>22 GPa), at least in basaltic systems (Wang and Takahashi, 1999). Overall, significant differences in $\delta^{41}\text{K}$ of the CLM and the BSE cannot be inferred from present data.

6. Summary of conclusions

(1) Non-metasomatized and lightly metasomatized, amphibole-bearing fertile lherzolites, the most common off-craton CLM rocks, show a narrow $\delta^{41}\text{K}$ range (-0.85 to -0.37‰ ; av. $-0.57 \pm 0.28\text{‰}$) overlapping the ranges for oceanic basalts and continental crust.

(2) The $\delta^{41}\text{K}$ values in xenolith-bearing alkali basalts and kimberlite ($-0.40 \pm 0.18\%$) as well as in mantle pyroxenites of magmatic origin ($-0.51 \pm 0.35\%$) are similar to $\delta^{41}\text{K}$ in oceanic basalts and continental magmatic rocks.

(3) Veined and strongly metasomatized mantle materials show a broader $\delta^{41}\text{K}$ range (-2.77 to 0.62%) than unaltered oceanic and continental magmatic rocks, likely due to (a) peculiar sources of metasomatic media that may contain recycled crustal materials, (b) kinetic isotope fractionation during local-scale interaction of mantle with melts and fluids.

(4) Andesite-hosted, amphibole-bearing harzburgites from the Kamchatka island arc show positive $\delta^{41}\text{K}$ ($0.51 \pm 0.31\%$) due to metasomatism by evolved, slab-derived fluids.

Acknowledgements

Brenna Tuller-Ross is thanked for the assistance in the clean lab. Some Tariat xenoliths were collected and studied jointly with R. Carlson, A.V. Golovin and O.B. Oleinikov collected samples from the Siberian craton, P. Plechov collected sample Av-50. KW acknowledges financial support from the McDonnell Center for the Space Sciences and NASA (Emerging Worlds Program grant number #80NSSC21K0379). We appreciate detailed and constructive comments of three anonymous reviewers and editorial handling of J. Blichert-Toft.

Figure Captions

Fig. 1. Element patterns for the REE, Rb and K normalized to primitive mantle (Hofmann, 1988) for whole-rock (WR, blue lines) samples and clinopyroxene (cpx, green lines) from this study. (A-B) Fertile, non-metasomatized spinel (A) and garnet-spinel (B) lherzolites (Carlson and Ionov, 2019; Ionov et al., 2005a). (C) Amphibole-bearing spinel lherzolites (Ionov et al., 1992b). (D) Feldspar-bearing lherzolites (Ionov et al., 1999; Ionov et al., 1995). (E) Harzburgites including cryptically metasomatized (Carlson and Ionov, 2019) and amphibole-bearing, subduction zone (Ionov, 2010) xenoliths. (F) Phlogopite-bearing harzburgites from the Siberian craton (Ionov et al., 2018). (G) Phlogopite-bearing peridotites from Tariat (Press et al., 1986). (H) Peridotites from Mongolia containing pockets of glass and micro-phenocrysts (melt-pockets) (Ionov et al., 1994).

Fig. 2. Histograms and probability density functions (PDF) for samples in this study. (A). All samples in this study compared to unaltered oceanic basalts (Tuller-Ross et al., 2019a). (B). Least altered fertile and lightly metasomatized lherzolites compared to unaltered oceanic basalts. (C). Discrete (Frey and Prinz, 1978) pyroxenites (Group 5a) and volcanic rocks hosting mantle xenoliths and related materials (Group 5b) compared to oceanic basalts. (D) Subduction zone harburgites (Group 3) compared to fertile and lightly metasomatized lherzolites and least altered oceanic basalts.

Fig. 3. K isotopic compositions of mantle-derived samples in this study and crustal samples from the literature. The lines for each group are averages \pm 1SD. Data sources: MORB (mid-ocean ridge basalt), OIB (ocean island basalt) and BABB (back-arc basin basalt), Tuller-Ross et al. (2019a); AOC (altered oceanic crust), Santiago Ramos et al. (2020); ophiolites, Parendo et al. (2017) and Santiago Ramos et al. (2020); eclogites, Liu et al. (2020); continental basalts, Sun et al. (2020); I-type, A-type, and S-type granites, Huang et al. (2020); loess and shales, Huang et al. (2020); pegmatites, Morgan et al. (2018); weathering profiles, Chen et al. (2020) and Teng et al. (2020). Grey-shaded areas are for the $\delta^{41}\text{K}$ ranges of oceanic basalts (left) and seawater.

Fig. 4. Covariation plots for $\delta^{41}\text{K}$ values vs. (A) K concentrations ($\mu\text{g/g}$) and (B) K/La ratios in WR samples in this study (Table 1). The plots show no robust correlations for any sample group or the whole suite.

Fig. 5. $\delta^{41}\text{K}$ values for composite xenoliths in this study. Blue circles are vein centers for phlogopite-rich veins in samples Mo-71 and 4334-1, and for bulk pyroxenite veins 4230-15v and 4399-24v. Red squares are phlogopites from margins of phlogopite vein 4334-1 and for veined peridotites Mo-71, 4230-15Lh and 4399-24Lh (Ionov et al., 1997; Ionov et al., 1998).

References

- Arevalo R., McDonough W. F. and Luong M. (2009) The K/U ratio of the silicate Earth: Insights into mantle composition, structure and thermal evolution. *Earth and Planetary Science Letters* **278**, 361-369.
- Bedini R. M. and Bodinier J.-L. (1999) Distribution of incompatible trace elements between the constituents of spinel peridotite xenoliths: ICP-MS data from the East African rift. *Geochimica et Cosmochimica Acta* **63**, 3883-3900.

- Bénard A., Klimm K., Woodland A. B., Arculus R. J., Wilke M., Botcharnikov R. E., Shimizu N., Nebel O., Rivard C. and Ionov D. A. (2018) Oxidising agents in sub-arc mantle melts link slab devolatilisation and arc magmas. *Nature Communications* **9**, 3500.
- Bénard A., Müntener O., Pilet S., Arculus R. J. and Nebel O. (2021) Silica-rich spinel harzburgite residues formed by fractional hybridization-melting of the intra-oceanic supra-subduction zone mantle: New evidence from TUBAF seamount peridotites. *Geochimica et Cosmochimica Acta* **293**, 477-506.
- Best M. G. (1974) Mantle-derived amphibole within inclusions in alkalic-basaltic lavas. *J. Geophys. Res.* **79**, 2107-2113.
- Bloom H., Lodders K., Chen H., Zhao C., Tian Z., Koefoed P., Pető M. K., Jiang Y. and Wang K. (2020) Potassium isotope compositions of carbonaceous and ordinary chondrites: Implications on the origin of volatile depletion in the early solar system. *Geochimica et Cosmochimica Acta* **277**, 111-131.
- Bodinier J.-L., Menzies M. A., Shimizu N., Frey F. A. and McPherson E. (2004) Silicate, hydrous and carbonate metasomatism at Lherz, France: contemporaneous derivatives of silicate melt-harzburgite reaction. *J. Petrol.* **45**, 299-320.
- Bodinier J.-L., Vasseur G., Vernières J., Dupuy C. and Fabriès J. (1990) Mechanisms of mantle metasomatism: geochemical evidence from the Lherz orogenic peridotite. *J. Petrol.* **31**, 597-628.
- Boyd F. R. and Nixon P. H. (1978) Ultramafic nodules from the Kimberley pipes, South Africa. *Geochimica et Cosmochimica Acta* **42**, 1367-1382.
- Carlson R. W. and Ionov D. A. (2019) Compositional characteristics of the MORB mantle and bulk silicate earth based on spinel peridotites from the Tariat Region, Mongolia. *Geochim. Cosmochim. Acta* **257**, 206-223.
- Chazot G., Menzies M. and Harte B. (1996) Silicate glasses in spinel lherzolites from Yemen: origin and composition. *Chem. Geol.* **134**, 159-179.
- Chen H., Liu X.-M. and Wang K. (2020) Potassium isotope fractionation during chemical weathering of basalts. *Earth and Planetary Science Letters* **539**, 116192.
- Chen H., Tian Z., Tuller-Ross B., Korotev R. L. and Wang K. (2019) High-precision potassium isotopic analysis by MC-ICP-MS: an inter-laboratory comparison and refined K atomic weight. *Journal of Analytical Atomic Spectrometry* **34**, 160-171.
- Dawson J. B. (1982) Contrasting types of mantle metasomatism. *Terra Cognita* **2**, 232.
- Dawson J. B. and Smith J. V. (1977) The MARID (mica-amphibole-rutile-ilmenite-diopside) suite of xenoliths in kimberlite. *Geochim. Cosmochim. Acta* **41**, 309-323
- Dawson J. B. and Smith J. V. (1982) Upper-mantle amphiboles: a review. *Mineral. Mag.* **45**, 35-46.
- Delaney J. S., Smith J. V., Carswell D. A. and Dawson J. B. (1980) Chemistry of micas from kimberlites and xenoliths: II. Primary- and secondary-textured micas from peridotite xenoliths. *Geochim. Cosmochim. Acta* **44**, 857-872.
- Delpech G., Gregoire M., O'Reilly S. Y., Cottin J. Y., Moine B., Michon G. and Giret A. (2004) Feldspar from carbonate-rich silicate metasomatism in the shallow oceanic mantle under Kerguelen Islands (South Indian Ocean). *Lithos* **75**, 209-237.
- Doucet L. S., Mattielli N., Ionov D. A., Debouge W. and Golovin A. V. (2016) Zn isotopic heterogeneity in the mantle: A melting control? *Earth and Planetary Science Letters* **451**, 232-240.
- Frey F. A. and Green D. H. (1974) The mineralogy, geochemistry and origin of lherzolite inclusions in Victorian basanites. *Geochim. Cosmochim. Acta* **38**, 1023-1059.
- Frey F. A. and Prinz M. (1978) Ultramafic inclusions from San Carlos, Arizona: Petrologic and geochemical data bearing on their petrogenesis. *Earth Planet Sci Lett* **38**, 129-176.

- Green D. H. and Wallace M. E. (1988) Mantle metasomatism by ephemeral carbonatite melts. *Nature* **336**, 459-462.
- Grégoire M., Bell D. R. and Le Roex A. P. (2002) Trace element geochemistry of phlogopite-rich mafic mantle xenoliths: their classification and their relationship to phlogopite-bearing peridotites and kimberlites revisited. *Contrib. Mineral. Petrol.* **142**, 603-625.
- Hart S. R. and Zindler A. (1986) In search of a bulk-Earth composition. *Chem. Geol.* **57**, 247-267.
- Hille M., Hu Y., Huang T.-Y. and Teng F.-Z. (2019) Homogeneous and heavy potassium isotopic composition of global oceans. *Science Bulletin* **64**, 1740-1742.
- Hiraga T., Anderson I. M. and Kohlstedt D. L. (2004) Grain boundaries as reservoirs of incompatible elements in the Earth's mantle. *Nature* **427**, 699-703.
- Hiraga T. and Kohlstedt D. (2009) Systematic distribution of incompatible elements in mantle peridotite: importance of intra- and inter-granular melt-like components. *Contrib. Miner. Petrol.* **158**, 149-167.
- Hofmann A. W. (1988) Chemical differentiation of the Earth: the relationship between mantle, continental crust, and oceanic crust. *Earth Planet Sci Lett* **90**, 297-314.
- Hofmann A. W. (1997) Mantle geochemistry: the message from oceanic volcanism. *Nature* **385**, 219-229.
- Hofmann A. W. (2003) Sampling mantle heterogeneity through oceanic basalts: isotopes and trace elements, in: Carlson, R.W. (Ed.), *Treatise on Geochemistry*. Vol. 2. The Mantle and Core. Elsevier, pp. 61-102.
- Hofmann A. W. and White W. M. (1982) Mantle plumes from ancient oceanic crust. *Earth Planet Sci Lett* **57**, 421-436.
- Hu Y., Chen X.-Y., Xu Y.-K. and Teng F.-Z. (2018) High-precision analysis of potassium isotopes by HR-MC-ICPMS. *Chem Geol* **493**, 100-108.
- Hu Y., Teng F.-Z. and Chauvel C. (2021a) Potassium isotopic evidence for sedimentary input to the mantle source of Lesser Antilles lavas. *Geochimica et Cosmochimica Acta* **295**, 98-111.
- Hu Y., Teng F.-Z., Helz R. T. and Chauvel C. (2021b) Potassium isotope fractionation during magmatic differentiation and the composition of the mantle. *J. Geophys. Res. Solid Earth* **126**, e2020JB021543.
- Hu Y., Teng F.-Z. and Ionov D. A. (2020a) Magnesium isotopic composition of metasomatized upper sub-arc mantle and its implications to Mg cycling in subduction zones. *Geochimica et Cosmochimica Acta* **278**, 219-234.
- Hu Y., Teng F.-Z., Plank T. and Chauvel C. (2020b) Potassium isotopic heterogeneity in subducting oceanic plates. *Science Advances* **6**, eabb2472.
- Huang T.-Y., Teng F.-Z., Rudnick R. L., Chen X.-Y., Hu Y., Liu Y.-S. and Wu F.-Y. (2020) Heterogeneous potassium isotopic composition of the upper continental crust. *Geochimica et Cosmochimica Acta* **278**, 122-136.
- Ionov D. A. (2010) Petrology of mantle wedge lithosphere: New data on supra-subduction zone peridotite xenoliths from the andesitic Avacha volcano, Kamchatka. *Journal of Petrology* **51**, 327-361.
- Ionov D. A., Ashchepkov I. and Jagoutz E. (2005a) The provenance of fertile off-craton lithospheric mantle: Sr-Nd isotope and chemical composition of garnet and spinel peridotite xenoliths from Vitim, Siberia. *Chem Geol* **217**, 41-75.
- Ionov D. A., Bénard A. and Plechov P. Y. (2011) Melt evolution in subarc mantle: evidence from heating experiments on spinel-hosted melt inclusions in peridotite xenoliths from the andesitic Avacha volcano (Kamchatka, Russia). *Contributions to Mineralogy and Petrology* **162**, 1159-1174.
- Ionov D. A., Blichert-Toft J. and Weis D. (2005b) Hf isotope compositions and HREE variations in off-craton garnet and spinel peridotite xenoliths from central Asia. *Geochimica et Cosmochimica Acta* **69**, 2399-2418.

Ionov D. A., Doucet L. S., Xu Y., Golovin A. V. and Oleinikov O. B. (2018) Reworking of Archean mantle in the NE Siberian craton by carbonatite and silicate melt metasomatism: Evidence from a carbonate-bearing, dunite-to-websterite xenolith suite from the Obnazhennaya kimberlite. *Geochimica et Cosmochimica Acta* **224**, 132-153.

Ionov D. A., Grégoire M. and Prikhod'ko V. S. (1999) Feldspar-Ti-oxide metasomatism in off-cratonic continental and oceanic upper mantle. *Earth and Planetary Science Letters* **165**, 37-44.

Ionov D. A., Hoefs J., Wedepohl K. H. and Wiechert U. (1992a) Content and isotopic composition of sulphur in ultramafic xenoliths from central Asia. *Earth Planet Sci Lett* **111**, 269-286.

Ionov D. A., Hofmann A. W., Merlet C., Gurenko A. A., Hellebrand E., Montagnac G., Gillet P. and Prikhodko V. S. (2006) Discovery of whitlockite in mantle xenoliths: Inferences for water- and halogen-poor fluids and trace element residence in the terrestrial upper mantle. *Earth and Planetary Science Letters* **244**, 201-217.

Ionov D. A., Hofmann A. W. and Shimizu N. (1994) Metasomatism-induced melting in mantle xenoliths from Mongolia. *J. Petrol.* **35**, 753-785.

Ionov D. A., Kramm U. and Stosch H. G. (1992b) Evolution of the upper mantle beneath the southern Baikal rift zone: a Sr-Nd isotope study of xenoliths from the Bartoy volcanoes. *Contrib. Mineral. Petrol.* **111**, 235-247.

Ionov D. A., O'Reilly S. Y. and Ashchepkov I. V. (1995) Feldspar-bearing lherzolite xenoliths in alkali basalts from Hamar-Daban, southern Baikal region, Russia. *Contrib. Mineral. Petrol.* **122**, 174-190.

Ionov D. A., O'Reilly S. Y. and Griffin W. L. (1997) Volatile-bearing minerals and lithophile trace elements in the upper mantle. *Chem. Geol.* **141**, 153-184.

Ionov D. A., O'Reilly S. Y. and Griffin W. L. (1998) A geotherm and lithospheric cross-section for central Mongolia, in: Flower, M.J.F., Chung, S.-L., Lo, C.-H., Lee, T.Y. (Eds.), *Mantle Dynamics and Plate Interactions in East Asia*. Amer. Geophys. Union, Geodynamics Ser. 27, Washington, DC, pp. 127-153.

Ionov D. A., Qi Y.-H., Kang J.-T., Golovin A. V., Oleinikov O. B., Zheng W., Anbar A. D., Zhang Z.-F. and Huang F. (2019) Calcium isotopic signatures of carbonatite and silicate metasomatism, melt percolation and crustal recycling in the lithospheric mantle. *Geochim. Cosmochim. Acta* **248**, 1-13.

Irving A. J. (1980) Petrology and geochemistry of composite ultramafic xenoliths in alkalic basalts and implications for magmatic processes within the mantle. *Am. J. Sci.* **280-A**, 389-426.

Kamenetsky V. S., Kamenetsky M. B., Golovin A. V., Sharygin V. V. and Maas R. (2012) Ultrafresh salty kimberlite of the Udachnaya–East pipe (Yakutia, Russia): A petrological oddity or fortuitous discovery? *Lithos* **152**, 173-186.

Kang J.-T., Ionov D. A., Liu F., Zhang C.-L., Golovin A. V., Qin L.-P., Zhang Z.-F. and Huang F. (2017) Calcium isotopic fractionation in mantle peridotites by melting and metasomatism and Ca isotope composition of the Bulk Silicate Earth. *Earth Planet Sci Lett* **474**, 128-137.

Kang J.-T., Ionov D. A., Zhu H.-L., Liu F., Zhang Z.-F., Liu Z. and Huang F. (2019) Calcium isotope sources and fractionation during melt-rock interaction in the lithospheric mantle: Evidence from pyroxenites, wehrlites, and eclogites. *Chem. Geol.* **524**, 272-282.

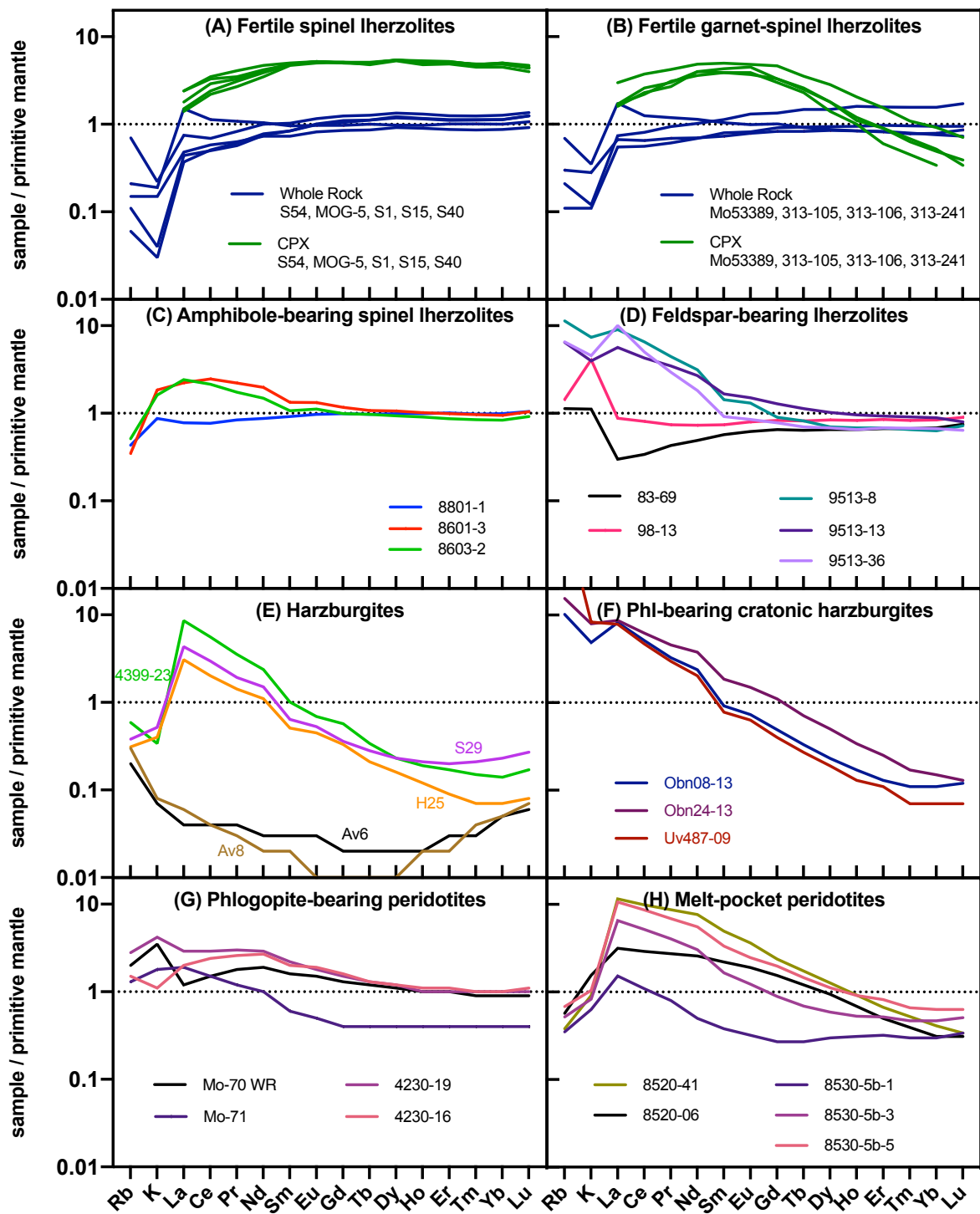
Kang J.-T., Zhou C., Huang J.-Y., Hao Y.-T., Liu F., Zhu H.-L., Zhang Z.-F. and Huang F. (2020) Diffusion-driven Ca-Fe isotope fractionations in the upper mantle: Implications for mantle cooling and melt infiltration. *Geochim. Cosmochim. Acta* **290**, 41-58.

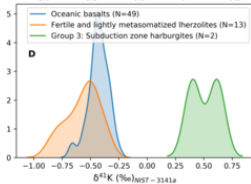
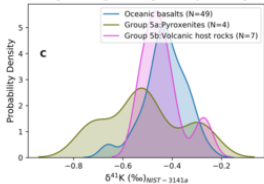
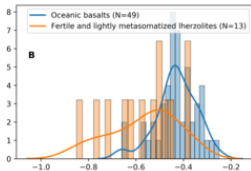
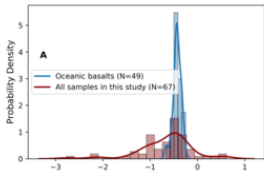
Li S., Li W., Beard B. L., Raymo M. E., Wang X., Chen Y. and Chen J. (2019a) K isotopes as a tracer for continental weathering and geological K cycling. *Proceedings of the National Academy of Sciences* **116**, 8740-8745.

- Li W., Beard B. L. and Li S. (2016) Precise measurement of stable potassium isotope ratios using a single focusing collision cell multi-collector ICP-MS. *Journal of Analytical Atomic Spectrometry* **31**, 1023-1029.
- Li Y., Wang W., Wu Z. and Huang S. (2019b) First-principles investigation of equilibrium K isotope fractionation among K-bearing minerals. *Geochimica et Cosmochimica Acta* **264**, 30-42.
- Liu H., Wang K., Sun W.-D., Xiao Y., Xue Y.-Y. and Tuller-Ross B. (2020) Extremely light K in subducted low-T altered oceanic crust: Implications for K recycling in subduction zone. *Geochimica et Cosmochimica Acta* **277**, 206-223.
- Liu H., Xue Y.-Y., Wang K., Sun W.-D. and Wang K. (2021) Contributions of slab-derived fluids to ultrapotassic rocks indicated by K isotopes. *Lithos* doi: 10.1016/j.lithos.2021.106202
- Lloyd F. E. and Bailey D. K. (1975) Light element metasomatism of the continental mantle: The evidence and the consequences. *Phys. Chem. Earth* **9**, 389-416.
- Lundstrom C. C., Chaussidon M., Hsui A. T., Kelemen P. and Zimmerman M. (2005) Observations of Li isotopic variations in the Trinity Ophiolite: Evidence for isotopic fractionation by diffusion during mantle melting. *Geochimica et Cosmochimica Acta* **69**, 735-751.
- Maaloe S. and Aoki K. I. (1977) The major element composition of the upper mantle estimated from the composition of lherzolites *Contrib. Mineral. Petrol.* **63**, 161-173
- Marschall H. R., Pogge von Strandmann P. A. E., Seitz H.-M., Elliott T. and Niu Y. (2007) The lithium isotopic composition of orogenic eclogites and deep subducted slabs. *Earth Planet Sci Lett* **262**, 563-580.
- McDonough W. F. (1990) Constraints on the composition of the continental lithospheric mantle. *Earth Planet Sci Lett* **101**, 1-18.
- McDonough W. F. and Sun S.-s. (1995) The composition of the Earth. *Chem Geol* **120**, 223-253.
- McDonough W. F., Sun S. S., Ringwood A. E., Jagoutz E. and Hofmann A. W. (1992) Potassium, rubidium and cesium in the Earth and Moon and the evolution of the mantle of the Earth. *Geochim. Cosmochim. Acta* **56**, 1001-1012.
- McNell A. M. and Edgar A. D. (1987) Sodium-rich metasomatism in the upper mantle: Implications of experiments on the Pyrolite-Na₂O-rich fluid system at 950°C, 20 kbar. *Geochim. Cosmochim. Acta* **51**, 2285-2294.
- Menzies M. A. and Hawkesworth C. J. (1987) *Mantle Metasomatism*. Academic Press, London, p. 500.
- Menzies M. A., Kempton P. and Dungan M. (1985) Interaction of continental lithosphere and asthenospheric melts below the Geronimo volcanic field, Arizona, U.S.A. *J. Petrol.* **26**, 663-693.
- Morgan L. E., Santiago Ramos D. P., Davidheiser-Kroll B., Faithfull J., Lloyd N. S., Ellam R. M. and Higgins J. A. (2018) High-precision 41K/39K measurements by MC-ICP-MS indicate terrestrial variability of $\delta^{41}\text{K}$. *Journal of Analytical Atomic Spectrometry* **33**, 175-186.
- Nakano T. and Fujii N. (1989) The multiphase grain control percolation: its implication for a partially molten rock. *J. Geophys. Res. Solid Earth* **94**, 15653-15661.
- Navon O. and Stolper E. (1987) Geochemical consequences of melt percolation: the upper mantle as a chromatographic column. *Journal of Geology* **95**, 285-307.
- Nielson J. E., Budahn J. R., Unruh D. M. and Wilshire H. G. (1993) Actualistic models of mantle metasomatism documented in a composite xenolith from Dish Hill, California. *Geochim. Cosmochim. Acta* **57**, 105-121.
- Palme H. and O'Neill H. S. C. (2003) Cosmochemical estimates of mantle composition, in: Carlson, R.W. (Ed.), *Treatise on Geochemistry*. Vol. 2. The Mantle and Core. Elsevier, pp. 1-38.
- Pareno C. A., Jacobsen S. B. and Wang K. (2017) K isotopes as a tracer of seafloor hydrothermal alteration. *Proceedings of the National Academy of Sciences* **114**, 1827-1831.

- Pogge von Strandmann P. A. E., Elliott T., Ionov D. and Niu Y. (2008) Li and Mg isotopes in the mantle: heterogeneity or diffusion? *Geochim. Cosmochim. Acta* **72**, A754.
- Pogge von Strandmann P. A. E., Elliott T., Marschall H. R., Coath C., Lai Y.-J., Jeffcoate A. and Ionov D. A. (2011) Variations of Li and Mg isotope ratios in bulk chondrites and mantle xenoliths. *Geochimica et Cosmochimica Acta* **75**, 5247-5268.
- Press S., Witt G., Seck H. A., Eonov D. and Kovalenko V. I. (1986) Spinel peridotite xenoliths from the Tariat Depression, Mongolia. I: Major element chemistry and mineralogy of a primitive mantle xenolith suite. *Geochimica et Cosmochimica Acta* **50**, 2587-2599.
- Richter F., Watson B., Chaussidon M., Mendybaev R. and Ruscitto D. (2014a) Lithium isotope fractionation by diffusion in minerals. Part 1: Pyroxenes. *Geochimica et Cosmochimica Acta* **126**, 352-370.
- Richter F. M., Bruce Watson E., Chaussidon M., Mendybaev R., Christensen J. N. and Qiu L. (2014b) Isotope fractionation of Li and K in silicate liquids by Soret diffusion. *Geochimica et Cosmochimica Acta* **138**, 136-145.
- Richter F. M., Dauphas N. and Teng F.-Z. (2009) Non-traditional fractionation of non-traditional isotopes: Evaporation, chemical diffusion and Soret diffusion. *Chem Geol* **258**, 92-103.
- Roden M. F. and Murthy V. R. (1985) Mantle Metasomatism. *Ann. Rev. Earth Planet. Sci.* **13**, 269-296.
- Rudnick R. L. and Ionov D. A. (2007) Lithium elemental and isotopic disequilibrium in minerals from peridotite xenoliths from far-east Russia: product of recent melt/fluid-rock reaction. *Earth Planet Sci Lett* **256**, 278-293.
- Salters V. J. M. and Stracke A. (2004) Composition of the depleted mantle. *Geochem. Geophys. Geosyst.* **5**, Q05004.
- Santiago Ramos D. P., Coogan L. A., Murphy J. G. and Higgins J. A. (2020) Low-temperature oceanic crust alteration and the isotopic budgets of potassium and magnesium in seawater. *Earth and Planetary Science Letters* **541**, 116290.
- Stosch H. G. and Seck H. A. (1980) Geochemistry and mineralogy of two spinel peridotite suites from Dreiser Weiher, West Germany. *Geochim. Cosmochim. Acta* **44**, 457-470.
- Strelow E. W. E., Von S. Toerien F. and Weinert C. H. S. W. (1970) Accurate determination of traces of sodium and potassium in rocks by ion exchange followed by atomic absorption spectroscopy. *Analytica Chimica Acta* **50**, 399-405.
- Sun J., Zhu X. K., Belshaw N. S., Chen W., Doroshkevich A. G., Luo W. J., Song W. L., Chen B. B., Cheng Z. G., Li Z. H., Wang Y., Kynicky J. and Henderson G. M. (2021) Ca isotope systematics of carbonatites: Insights into carbonatite source and evolution. *Geochemical Perspectives Letters* **17**, 11-15.
- Sun Y., Teng F.-Z., Hu Y., Chen X.-Y. and Pang K.-N. (2020) Tracing subducted oceanic slabs in the mantle by using potassium isotopes. *Geochimica et Cosmochimica Acta* **278**, 353-360.
- Teng F.-Z., Dauphas N. and Watkins J. M. (2017) Non-traditional stable isotopes: Retrospective and prospective. *Reviews in Mineralogy and Geochemistry* **82**, 1-26.
- Teng F.-Z., Hu Y., Ma J.-L., Wei G.-J. and Rudnick R. L. (2020) Potassium isotope fractionation during continental weathering and implications for global K isotopic balance. *Geochimica et Cosmochimica Acta* **278**, 261-271.
- Teng F.-Z., McDonough W. F., Rudnick R. L. and Wing B. A. (2007) Limited lithium isotopic fractionation during progressive metamorphic dehydration in metapelites: A case study from the Onawa contact aureole, Maine. *Chem. Geol.* **239**, 1-12.
- Toramaru A. and Fujii N. (1986) Connectivity of melt phase in a partially molten peridotite. *J. Geophys. Res.* **91**, 9239-9252.

- Tuller-Ross B., Marty B., Chen H., Kelley K. A., Lee H. and Wang K. (2019a) Potassium isotope systematics of oceanic basalts. *Geochimica et Cosmochimica Acta* **259**, 144-154.
- Tuller-Ross B., Savage P. S., Chen H. and Wang K. (2019b) Potassium isotope fractionation during magmatic differentiation of basalt to rhyolite. *Chem Geol* **525**, 37-45.
- Wang K., Close H. G., Tuller-Ross B. and Chen H. (2020) Global average potassium isotope composition of modern seawater. *ACS Earth and Space Chemistry* **4**, 1010-1017.
- Wang K. and Jacobsen S. B. (2016) An estimate of the Bulk Silicate Earth potassium isotopic composition based on MC-ICPMS measurements of basalts. *Geochimica et Cosmochimica Acta* **178**, 223-232.
- Wang W. and Takahashi E. (1999) Subsolidus and melting experiments of a K-rich basaltic composition to 27 GPa: Implication for the behavior of potassium in the mantle. *Amer. Mineralogist* **84**, 357-361.
- Wang Y., Foley S. F. and Prelević D. (2017) Potassium-rich magmatism from a phlogopite-free source. *Geology* **45**, 467-470.
- Watkins J. M., DePaolo D. J. and Watson E. B. (2017) Kinetic Fractionation of Non-Traditional Stable Isotopes by Diffusion and Crystal Growth Reactions. *Reviews in Mineralogy and Geochemistry* **82**, 85-125.
- Weyer S. and Ionov D. A. (2007) Partial melting and melt percolation in the mantle: The message from Fe isotopes. *Earth and Planetary Science Letters* **259**, 119-133.
- Wiechert U., Ionov D. A. and Wedepohl K. H. (1997) Spinel peridotite xenoliths from the Atsagin-Dush volcano, Dariganga lava plateau, Mongolia: A record of partial melting and cryptic metasomatism in the upper mantle. *Contrib. Mineral. Petrol.* **126**, 345-364.
- Witt-Eickschen G. and Kramm U. (1998) Evidence for the multiple stage evolution of the subcontinental lithospheric mantle beneath the Eifel (Germany) from pyroxenite and composite pyroxenite/peridotite xenoliths. *Contrib. Mineral. Petrol.* **131**, 258-272.
- Wu H., He Y., Teng F.-Z., Ke S., Hou Z. and Li S. (2018) Diffusion-driven magnesium and iron isotope fractionation at a gabbro-granite boundary. *Geochimica et Cosmochimica Acta* **222**, 671-684.
- Xia J., Qin L., Shen J., Carlson R. W., Ionov D. A. and Mock T. D. (2017) Chromium isotope heterogeneity in the mantle. *Earth and Planetary Science Letters* **464**, 103-115.
- Xu Y. G., Mercier J.-C. C., Menzies M. A., Ross J. V., Harte B., Lin C. and Shi L. (1996) K-rich glass-bearing wehrlite xenoliths from Yitong, northeastern China: petrological and chemical evidence for mantle metasomatism. *Contrib. Mineral. Petrol.* **125**, 406-420.
- Yaxley G. M., Green D. H. and Kamenetsky V. (1998) Carbonate metasomatism in the southeastern Australian lithosphere. *J. Petrol.* **39**, 1917-1931.
- Zeng H., Rozsa V. F., Nie N. X., Zhang Z., Pham T. A., Galli G. and Dauphas N. (2019) Ab Initio calculation of equilibrium isotopic fractionations of potassium and rubidium in minerals and water. *ACS Earth and Space Chemistry* **3**, 2601-2612.
- Zibera L., Klemme S. and Nimis P. (2013) Garnet and spinel in fertile and depleted mantle: insights from thermodynamic modelling. *Contributions to Mineralogy and Petrology* **166**, 411-421.
- Zinngrebe E. and Foley S. (1995) Metasomatism in mantle xenoliths from Gees, West Eifel, Germany: evidence for the genesis of calc-alkaline glasses and metasomatic Ca-enrichment. *Contrib. Mineral. Petrol.* **122**, 79-96.

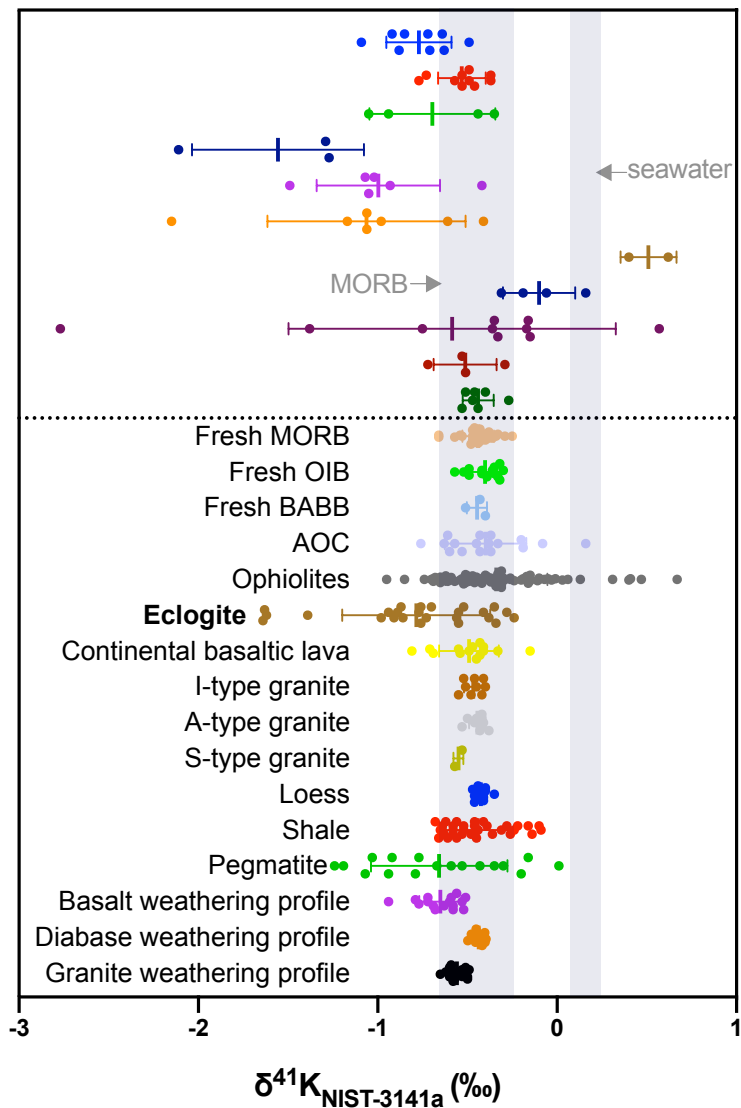


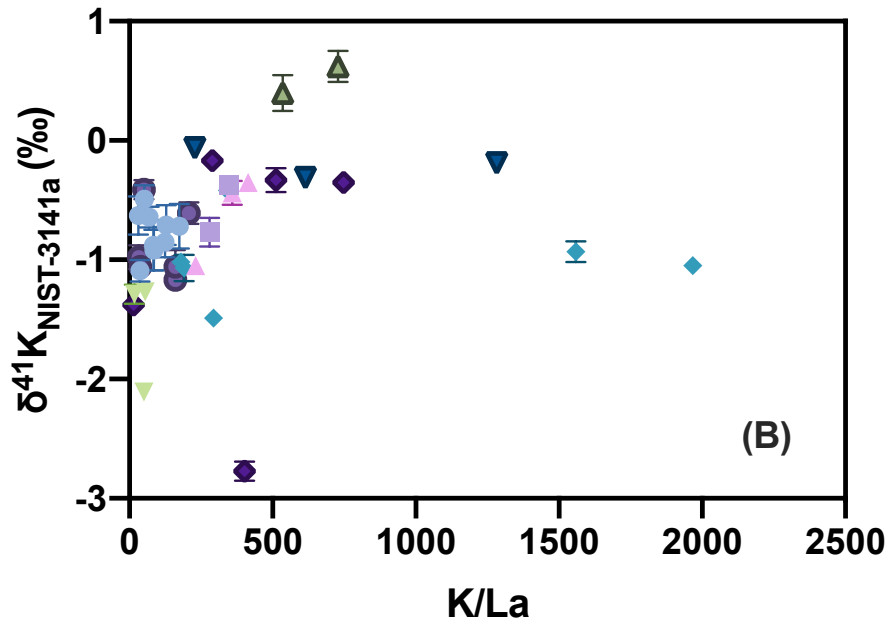
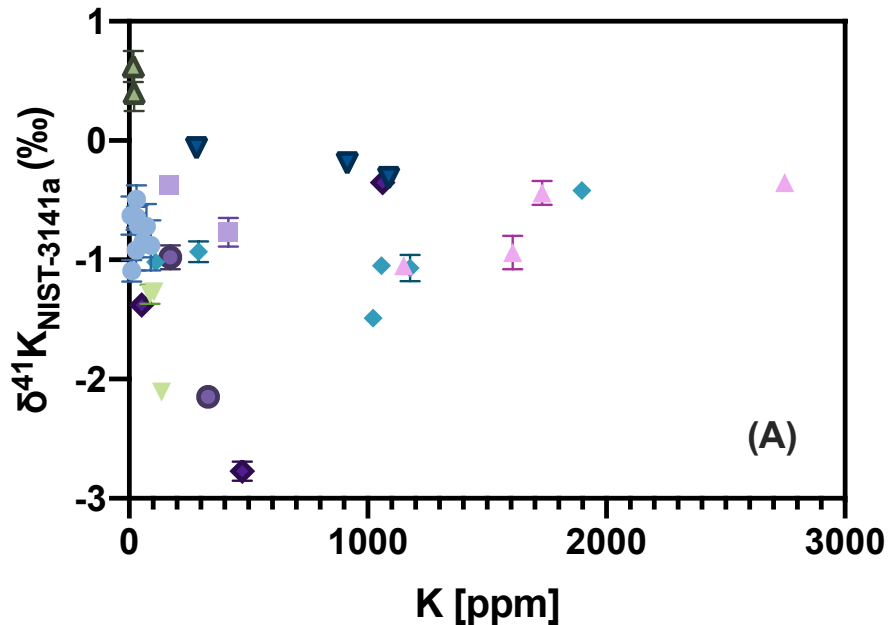


Mantle
(This study)

- Group 1. Fertile lherzolites (Lh)
- Group 2a. Lightly metasomatized Lh
- Group 2b. Phl-bearing cratonic Hzb
- Group 2c. Cryptically metasomatized Hzb
- Group 2d. Metasomatized, Kfs-bearing Lh
- Group 2e. Melt-pocket Lh/Hb
- Group 3. Subduction zone Hzb**
- Group 4a. Modally heterogeneous Lh
- Group 4b. Composite xenoliths
- Group 5a. Pyroxenites
- Group 5b. Volcanic host rocks

Crust
(Literature)





- Group 1. Fertile lherzolites (Lh)
- Group 2a. Lightly metasomatized Lh
- ▲ Group 2b. Phl-bearing cratonic Hzb
- ▼ Group 2c. Cryptically metasomatized Hzb
- ◆ Group 2d. Metasomatized, Kfs-bearing Lh

- Group 2e. Melt-pocket Lh/Hb
- ▲ Group 3. Subduction zone Hzb
- ▼ Group 4a. Modally heterogeneous Lh
- ◆ Group 4b. Composite xenoliths

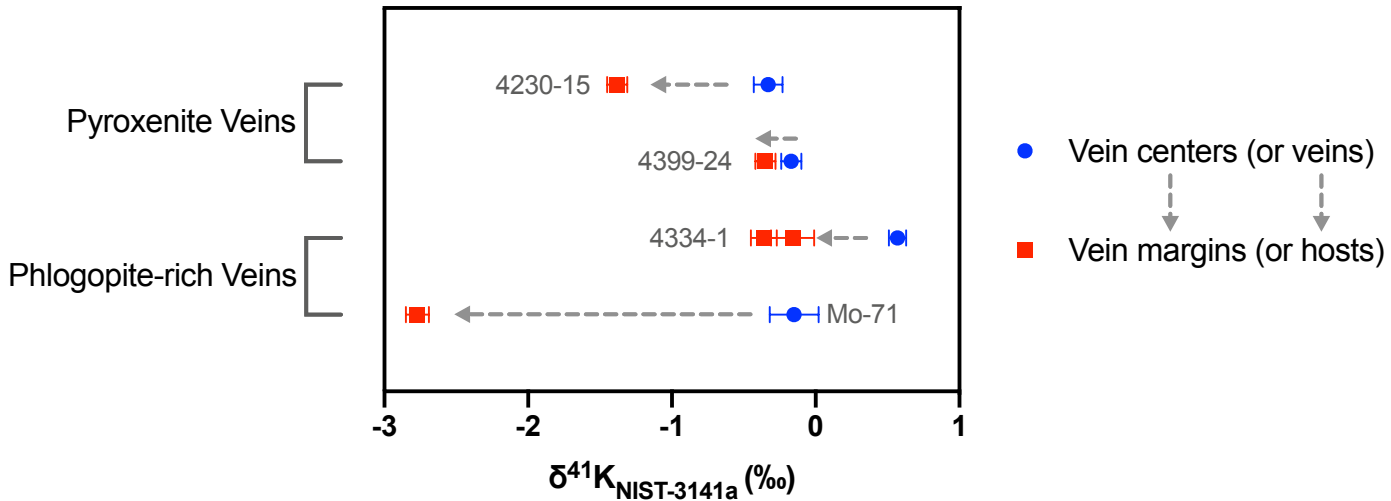


Table 1. Potassium concentration, isotopic composition and a summary of essential data for samples in this study

Sample N°	Locality	Sample type	Rock type	Al ₂ O ₃ WR	Mg#	Liter.	K, µg/g	K/La	δ ⁴¹ K	2sd	n
PM (BSE)											
		WR		4.45	0.893	240		370			
Group 1. Fertile to moderately melt-depleted spinel and garnet hercynites (low-K, lo											
554*	Shava, Tariat	WR	Fertile sp Lh	4.47	0.895	/s80/	57	124	-0.85	0.13	10
MOG-5*	..	WR	..	4.35	0.893		48	31	-0.49	0.12	10
S1*	..	WR	..	4.27	0.891	/s80/	7	31	-0.63	0.16	5
S15	..	WR	..	4.00	0.898	/s80/	10	37	-1.09	0.09	5
S40	..	WR	..	3.43	0.901	/s80/	38	129	-0.71	0.17	10
<i>Averages, spinel Lh:</i>											
				4.10	0.896		29	74	-0.75	0.45	
Mos3389*	Shava, Tariat	WR	Fertile gar-sp Lh	4.70	0.892	/s80/	31	69	-0.64	0.09	7
313-105	Vitim, BR	WR	..	3.23	0.899	105	72	174	-0.72	0.19	10
313-106	..	WR	..	3.42	0.895	/s80/	90	84	-0.88	0.21	9
313-241	..	WR	..	3.84	0.895	/s80/	29	86	-0.92	0.17	11
<i>Averages, garnet Lh:</i>											
				3.80	0.895		56	103	-0.79	0.26	
Group 2. Metasomatized, modally homogeneous intra-plate peridotites											
<i>Group 2a. Lightly metasomatized hercynites with accessory amphibole ± phlogopite</i>											
8801-1	Bartoy, BR	WR	Fertile Lh, 2% am	3.88	0.891	225	166	348	-0.37	0.07	12
8603-2	..	WR	Fertile Lh, ~4% am	3.90	0.899	475	416	280	-0.77	0.12	12
8603-2am	..	Am	..	-	0.885	14110	14565		-0.73	0.09	12
Bar-7am	..	Am	Thin vein	-	-	14025	2058		-0.49	0.09	12
313-114am	Vitim, BR	Am	..	-	-	15350	11005		-0.46	0.18	12
313-103am	..	Am	..	-	0.867	15850	4615		-0.57	0.08	12
313-103phl	..	Phi+Am	..	-	0.881	-	13788		-0.53	0.09	12
8505-2	SE Mongolia	WR	Phi-sp low-cpx Lh	-	-	-	3659		-0.49	0.07	12
40-1am	Germany	Am	Am-peridotite	-	-	11780	10339		-0.37	0.12	12
Gn-1am	SE Australia	Am	..	-	-	-	4862		-0.53	0.13	12
<i>Averages:</i>											
				3.89	0.885		291	314	-0.53	0.26	
<i>Group 2b. Phlogopite-bearing cratonic harzburgites</i>											
Obn08-13	Siber. craton	WR	Phi-Carb-Gar Hb	1.20	0.919	1162	1150	231	-1.05	0.07	12
Obn24-13	..	WR	..	0.41	0.918	1909	1731	359	-0.44	0.10	11
Uv487-09	..	WR	Phi-Sp Hb	0.19	0.919	-	2747	414	-0.35	0.05	12
Uv98-13	..	WR	Phi-Amph Hb	-	-	-	1607		-0.94	0.14	12
<i>Averages:</i>											
				0.60	0.919		1809	335	-0.69	0.70	
<i>Group 2c. Cryptically metasomatized harzburgites</i>											
4399-23	Shava, Tariat	WR	Sp Hb	0.88	0.912	134	88	17	-1.29	0.08	9
S29	..	WR	..	0.90	0.915	/160/	135	51	-2.11	0.07	12
H25	Haer, Tariat	WR	..	0.62	0.918	/80/	104	55	-1.27	0.05	12
<i>Averages:</i>											
				0.80	0.915		109	41	-1.56	0.96	
<i>Group 2d. Metasomatized, feldspar-bearing hercynites</i>											
9512-5	Barhatny	WR	Sp Lh, trace Fs	1.97	0.898	133	111	180	-1.02	0.05	11
9513-8	..	WR	Sp Lh, Fs veins	2.53	0.894	2116	1898	343	-0.42	0.07	12
9513-13	..	WR	..	3.45	0.894	1303	1023	294	-1.49	0.07	12
9513-36	..	WR	..	2.72	0.897	1402	1178	191	-1.07	0.11	12
83-69	Hamar, BRZ	WR	Sp Lh, Fs pockets	3.27	0.899	375	290	1559	-0.93	0.09	12
98-13	..	WR	..	3.62	0.897	683	1057	1968	-1.05	0.06	12
<i>Averages:</i>											
				2.93	0.897		926	756	-1.00	0.69	
<i>Group 2e. Melt-pocket peridotites (pockets of glass with late-stage cpx, ol and sp)</i>											
8520-6mp	SE Mongolia	Glass	Gl-cpx-sp pocket	/1/	/0.907/	3485	2911	207	-0.61	0.09	12
8520-41	..	WR	Melt-pocket Hb	1.16	0.910	234	172	33	-0.98	0.10	12
8525-1	..	WR	..	1.31	0.900	390	330		-2.15	0.06	12
8530-5b-1a	Shava, Tariat	WR	Lh, spongy-rim cpx	1.88	0.905	<80	41	160	-1.17	0.13	10
8530-5b-1a (duplicate)	..	WR	53	207	-1.12	0.35	12
8530-5b-1b	..	WR	80	240	-1.06	0.28	9
8530-5b-3	..	WR	Lh, spongy cpx, Gl	2.03	0.905	<80	50	50	-0.41	0.16	10
8530-5b-5	..	WR	Lh, melt pockets	1.98	0.902	/170/	38	38	-1.06	0.10	10
<i>Averages:</i>											
				1.67	0.904		134	134	-1.07	0.51	

Table 1 continued

Sample N°	Locality	Sample type	Rock type	Al ₂ O ₃ WR	Mg#	Liter.	K, µg/g	K/La	δ ⁴¹ K	2sd	n
Group 3. Subduction zone harzburgites (active plate margin, Kamchatka)											
Av-6	Avacha	WR	Hb, 0.9% am	0.48	0.909	-	17	728	0.62	0.13	11
Av-8	..	WR	Hb, 0.7% am	0.78	0.911	-	21	535	0.40	0.15	11
<i>Averages:</i>											
				0.63	0.910		19	632	0.51	0.31	
Group 4. Modally heterogeneous, metasomatized mantle											
<i>Group 4a. Hercynites with phi-rich domains</i>											
Mo-70	Shava, Tariat	WR	Phi-Lherzolite	3.84	0.891	996	914	1283	-0.19	0.06	12
4230-19	..	WR	..	3.92	0.890	1245	1087	614	-0.31	0.07	12
4230-16	..	WR	..	4.32	0.887	390	282	228	-0.06	0.06	12
4230-16phl	..	Phi	..	-	0.904	-	0.904	-	0.16	0.07	11
<i>Averages:</i>											
				4.03	0.893		843	708	-0.10	0.20	
<i>Group 4b. Composite xenoliths: Phi-rich and pyroxenite veins in peridotites</i>											
Mo-71host	Shava, Tariat	WR	Lh, host of Phi vein	2.22	0.901	581	474	402	-2.77	0.08	12
Mo-71 vein	..	Phi	Coarse vein Phi	-	-	-	-	-	-0.15	0.17	9
4334-1b	..	Phi	Phi vein margin	-	-	80330	-	-	-0.16	0.15	8
4334-1g	..	Phi	Phi vein inside	-	-	81410	-	-	-0.36	0.09	8
4334-1u	..	Phi	Phi-cpx vein center	-	-	80000	50228	-	0.57	0.06	12
4230-15Lh	Shava, Tariat	WR	Lh, host to vein	3.37	0.911	87	52	15	-1.38	0.07	11
4230-15v	..	WR	Phi-Sp pyroxenite	11.2	0.904	2800	2327	512	-0.33	0.10	12
4399-24Lh	..	WR	Phi-Sp Lh, host	3.75	0.896	1220	1062	748	-0.35	0.07	12
4399-24v	..	WR	Gar-opx-te vein	12.3	0.878	340	228	290	-0.17	0.07	12
8530-15	..	Phi	Coarse vein Phi	-	-	80750	-	-	-0.75	0.16	8
<i>Average</i>											
								0.83	-0.59	1.82	
Group 5. Pyroxenites and mantle-derived volcanic rocks											
<i>Group 5a. Pyroxenites</i>											
4230-18	Shava, Tariat	WR	Gar-Cpx-te	13.5	0.85	-	383	-	-0.72	0.12	12
4399-7	..	WR	Phi-Opx-te	5.28	0.80	3040	2708	-	-0.29	0.07	12
8530-81	..	WR	Black Phi-Opx-te	-	-	14750	13039	-	-0.53	0.09	12
8530-81phl	..	Phi	Phi separate	-	-	-	66377	-	-0.51	0.05	12
Mo-60	Shava, Tariat	WR	Crustal granulite	18.6	0.48	7333	-	-	-0.53	0.25	9
<i>Average</i>											
									-0.51	0.17	
<i>Group 5b. Volcanic rocks hosting mantle xenoliths and related materials</i>											
K-27-04	Siber. craton	WR	Kimberlite	1.53	0.88	4150	4746	-	-0.40	0.07	11
Mo-23	Shava, Tariat	WR	Vesicular lava	14.4	0.62	34025	30506	585	-0.47	0.15	12
4230-6a	..	Phi	Phi megacryst	15.1	0.59	74700	61850	-	-0.46	0.10	12
4230-1	..	WR	Black basaltic Gl	15.5	0.41	41500	29733	-	-0.27	0.14	12
Av-18	Avacha	WR	Am-rich selvage	-	-	-	-	-	-0.53	0.27	11
Av-18 cryst	..	Am	..	-	0.72	-	-	-	-0.51	0.38	22
Av-50selv	..	Am	..	-	0.72	-	-	-	-0.44	0.32	21
<i>Average</i>											
									-0.44	0.17	

Liter, K content from literature data obtained with AAS in whole-rocks (Ionov et al., 1992) and EPMA in minerals

(Ionov et al., 1997); values in parentheses are estimates for low K concentrations obtained with XRF.

WR, whole-rock; sd, standard deviation; BR, Baikal region; Lh, hercynite; Hb, harzburgite; Fs, feldspar; Sp, spinel;

Am, amphibole; Phi, phlogopite; Gl, silicate glass; Gar, garnet; Opx-te, orthopyroxenite; Cpx-te, clinopyroxenite.

*Samples that may be close in chemical composition to the primitive mantle (PM, equivalent of the Bulk Silicate Earth, BSE).